Interpretable Domain Adaptation Using Unsupervised Feature Selection on Pre-trained Source Models

Luxin Zhang, Pascal Germain, Yacine Kessaci, Christophe Biernacki

Interpretable Domain Adaptation Using Unsupervised Feature Selection on Pre-trained Source Models

Luxin Zhang [*1], Pascal Germain [†3], Yacine Kessaci [‡1], and Christophe Biernacki [§2]

[1]Worldline Labs, France
[2]Inria, Université de Lille, CNRS, France
[3]Université Laval, Canada

Abstract

We study a realistic domain adaptation setting where one has access to an already existing "black-box" machine learning model. Indeed, in real-life scenarios, an efficient pre-trained source domain predictive model is often available and required to be preserved. The solution we propose to this problem has the asset of providing an interpretable *target to source* transformation by seeking a sparse and ordered *coordinate-wise* adaptation of the feature space in addition to elementary mapping functions. To automatically select the subset of features to be adapted, we first introduce a weakly-supervised process relying on scarce labeled target data. Then, we address a more challenging unsupervised version of this domain adaptation scenario. To this end, we propose a new pseudo-label estimator over unlabeled target examples, which is based on rank-stability in regards to the source model prediction. Such estimated "labels" are further used in a feature selection process to assess whether each feature needs to be transformed to achieve adaptation. We provide theoretical foundations of our method as well as an efficient implementation. Numerical experiments on real datasets show particularly encouraging results since approaching the supervised case, where one has access to labeled target samples.

1 Introduction

Domain adaptation (DA) methods deal with a scenario where training data, the so-called source domain data, and test data, the so-called target domain data,

[*]luxin.zhang@worldlne.com
[†]pascal.germain@ift.ulaval.ca
[‡]yacine.kessaci@worldline.com
[§]christophe.biernacki@inria.fr

are drawn from different distributions [47, 63]. This is a ubiquitous challenge in industrial machine learning applications. For example, to expand companies' businesses, a payment fraud detection system trained in one geographical localization, say one country (source domain), may be used to detect fraudsters in another country (target domain) where people have different payment habits. Directly training such a predictive model in a new country is not desirable since one has scarce labeled target domain data. However, abundant unlabeled data are usually easy to get. Classical DA methods address this problem often by seeking a latent space where input distributions of target and source domains coincide [46, 1] or by transforming source domain data to match distributions of the target domain [60, 61]. Current approaches based on deep neural networks rely on adversarial learning to generate domain invariant features [18, 65]. However, such methods require retraining a predictive model after or during the adaptation, which is undesirable in a real-life industrial setting. Indeed, in many real-life scenarios, a well-performing pre-trained source domain predictive model is often given. The pre-trained predictive model can be from various model types: neural networks, decision trees, and expert rules, to name a few. Retraining such an aggregation of models requires tedious hyper-parameter fine-tuning and can be even unfeasible due to no longer accessible expertise. As a result, it is natural to consider this pre-trained model as a "black-box" and reuse it directly. Furthermore, the automatically generated features by deep neural networks are generally not interpretable; hence provide no insights to understand drifts between source and target domains. Alternatively, we propose to stand in a *target to source* DA scenario: one transforms target data into the source ones and predicts target domain labels using the pre-trained source model directly without supplementary retraining. Moreover, we focus on the adaptation problem of tabular data where the input space contains categorical attributes as well as numerical ones, thus complexifying the analysis. All these constraints require the adaptation method to be predictive *model-agnostic*, *retraining-free*, and *feature-type independent*.

To address such a challenging *target to source* DA scenario, we propose to use *coordinate-wise* optimal transports for adaptation (note that we initiated this line of research in an early conference paper [78]). As we show further in experiments, transformation functions of *coordinate-wise* optimal transports are easily interpretable and can seamlessly adapt numerical features as well as categorical ones. Moreover, leveraging a weakly-supervised feature selection process, we enhanced our method's interpretability and prediction performance by providing a sparse and ordered transformation function. More precisely, we ranked features of input space by their contributions to DA tasks and focused on the adaptation of features with the most contributions. From a business point of view, the selected small subset of features can reveal the source of gaps between source and target domains and provides business experts, with or without machine learning backgrounds, with interpretability to gain more insights for a better understanding of different domains. Although our previous proposed method empirically achieved state-of-the-art performances over several real-life DA tasks, a small subset of labeled target data is required during the

Table 1: Comparison of different DA methods. (i) *classical adaptation method*: SA [15], (ii) *deep adaptation methods*: DANN [18], (iii) *classical adaptation method* with feature selection: OT Feature Selection [19].

Advantages	SA	DANN	OT Feature Selection	**Ours**
Model-Agnostic	✓	✗	✓	✓
Retraining-Free	✗	✗	✗	✓
Feature-type Free	✗	✓	✗	✓
Huge Dataset	✗	✓	✗	✓
Interpretable	✓	✗	✓	✓

feature selection process; thus, we were in a weakly-supervised DA scenario. However, in practice, target domain labels are often missing, limiting the previous method's spectrum of use.

We extend this DA method, typically the idea of feature selection over pre-trained source models, to an unsupervised DA setting through a general DA pipeline. Our main contributions are: (i) We propose a new unsupervised DA function leveraging the stability of ranks of predictions to select and adapt the features that contribute the most to DA tasks. (ii) We provide theoretical foundations of the proposed unsupervised feature selection method and give an efficient implementation. (iii) We represent our method over challenging DA tasks via interpretable illustrations empirically.

We organize the paper as follows. Section 2 reviews some classical setting DA methods and some pseudo-labeling techniques. Section 3 gives the formalization of the *target to source* DA problem and introduces our pipeline of DA. We propose our unsupervised feature selection method in Section 4 in addition to its theoretical foundations. Section 5 provides an efficient implementation of our method. In Section 6, we empirically evaluate our proposition on the Amazon review benchmark and two challenging real-life fraud detection tasks. Finally, we conclude and give some future perspectives in Section 7.

2 Related Work

2.1 Domain Adaptation (DA)

According to classes of transformation functions, DA methods can be roughly categorized as *deep adaptation methods* that rely on deep neural networks and *classical adaptation methods* that do not use neural networks to adapt data.

Deep adaptation methods are shown to be capable of extracting transferable features between different tasks [73]. Recent *deep adaptation methods* enhance this transferability by plugging into neural networks an adaptation layer [40, 20, 43] to minimize Maximum Mean Discrepancy (MMD) or other statistical moments of different orders [76, 7] between source and target distributions.

Another popular paradigm relies on adversarial learning [21] to generate domain invariant features [18, 65, 41, 55, 67]. Besides, [33] proposes to use early exiting and residual blocks skipping to accelerate the inference process. Since a perfect alignment directly between source and target domain is difficult to achieve, [13] proposes the concept of "bridge" to gradually align source and target representations in an intermediate domain and simplify the optimization of the domain discriminator. [12] considers domain-specific characteristics as heuristic representations and leverages heuristic search perspectives to minimize domain discrepancies gradually. Wei et al. have pointed out that the objective of domain alignment may not coordinate with the classification tasks. They propose to leverage meta-optimization strategies [69] and feature decompositions [70] to mitigate such an inconsistency problem. The proposed method has achieved state-of-the-art adaptation performance on various image benchmarks. Note that all these methods project source and target data into a common latent space and require retraining the predictive model. These approaches are not desirable when a "black-box" pre-trained model is given and cannot be retrained due to the manual defined expert rules, which is the case in our problem.

Source-free DA [28, 34, 35, 29, 72] and *"black-box" DA* [36, 77] share the same idea of leveraging pre-trained source domain predictive models like ours. The former supposes the source domain data are not available, while one has full access to pre-trained source domain predictive models. The latter considers the pre-trained source domain model as a "black-box", and only the input-output responses of pre-trained models are available. Standing in a source-free DA setting, [23] adopts a contrastive learning schema and relies on historical source domain classifiers to build a consistent target representation. [32] tackles a more challenging task where either source domain data or the target domain data are unknown and proposes a novel adversarial-attack-based method to address the DA problem. Faced with a "black-box" DA setting, [64] proposes reprogramming model outputs using a few labeled target domain data. [38] focuses on the label shift problem where source and target domain output distributions differ. [36] distills knowledge from the source domain with interpolation consistency training and mutual information maximization. It requires a smoothing regularization when training the "black-box" model. However, all these methods do not address our problem, as our proposition focuses on adapting tabular data in an unsupervised setting and has no restriction over the structure or family of predictive models. In our "black-box" setting, source domain models can be of any type (*e.g.*, decision trees, expert rules, etc.). Besides, we have access to source domain data so that our adaptation method can apply to generic "black-box" predictive models. Although many methods leverage the flexibility of deep neural networks and advance in stochastic optimization methods to address complex DA settings such as partial DA [5, 6], open set DA[48, 56], and universal DA [74, 31]. This paper mainly focuses on a non-neural network limited, model-agnostic closed set DA problem. Indeed, deep neural networks are powerful for extracting representations, while for machine learning tasks with hand-crafted tabular data, tree-based models are still state of the art [4]. Moreover, deep neural networks, especially adversarial networks, are challenging

to train and need lots of manual tuning to find the optimal hyper-parameter and trade-off between classification and adversarial losses or regularization terms. Such hyper-parameter searching is not straightforward in an unsupervised DA scenario [75]. Our proposition exceeds *deep adaptation methods* by generalizing to all families of predictive models.

Classical adaptation methods focus mainly on the transformation of hand-crafted features. Some well-known methods address the DA problem by minimizing measures like Kullback-Leibler Divergence [58, 60] or MMD [46, 1, 42] between source and target domain distributions. Others align target and source domain correlation matrices [61] or principal axes [15]. Recent research works that leverage optimal transport theory [44, 26] and advances in computational optimal transport [14] consider the DA problem as finding the optimal transport plan between source and target domains [50, 11, 10]. However, most of these methods are not scalable to transform massive datasets or fail to adapt categorical features.

2.2 Feature selection and DA

To take into account both interpretability and a huge dataset of mixed feature types, our proposition leverages a *coordinate-wise* transformation [78] and feature selection DA methods [57, 66, 19]. Classical feature selection DA methods predict target labels relying solely on selected domain invariant features. However, label-relevant features could be discarded and decrease prediction performance. Alternatively, we keep all features such that one can directly use pre-trained source models to predict target labels. In addition, features that contribute to DA are adapted to mitigate gaps between source and target domains. Besides, the selected features by the unsupervised method offer an immediate overview of the source of drifts between domains.

2.3 Pseudo-labeling and DA

The pseudo-labeling method is first used to guess and annotate unlabeled data in semi-supervised learning [81]. Namely, one iteratively trains a model with real and pseudo-labels and updates pseudo-labels using the most confident predictions. In an unsupervised DA scenario, one annotates unlabeled target data using the most confident predictions of source models [30]. Leveraging this technique, Long et al. [41] propose to align target and source domain conditional distributions for DAs. Some other works [8, 54] combine co-training or tri-training techniques to get estimations of pseudo-labels of target domains. In [17] and [59], the authors use a teacher network to predict target labels and refine decision boundaries. Different from the aforementioned methods that use discrete class labels with the most confident predictions as pseudo-labels, Wang and Breckon [68] and Motiian et al. [45] adopt soft pseudo-labels for adaptation tasks. Inspired by the success of soft pseudo-labeling methods, we propose a new pseudo-label estimator relying on rank stability of predictions that helps select features that contribute the most to DA tasks. Our approach gives probability scores that unlabeled examples

belong to one class, representing more precisely inter-example relationships than just class labels, especially when classes are highly unbalanced (more details in Section 4). Table 1 highlights the added values of our proposition compared to some typical adaptation methods.

3 Target to Source Domain Adaptation

We first introduce the formalization of the *target to source* DA scenario and some basic notations. Of note, the current section essentially recaps the framework we previously introduced for the weakly-supervised setting [78], on which we build the contribution of the forthcoming Section 4 for unsupervised feature selection.

The objective of the *target to source* DA consists of finding a predictive model independent transformation $\mathcal{G} : \mathcal{X} \to \mathcal{X}$ that aligns input marginal distributions and output conditional distributions between source and target domains, that is,

$$\begin{cases} P(X^s) = P(\mathcal{G}(X^t)) \,, \\ P(Y^s|X^s) = P(Y^t|\mathcal{G}(X^t)) \,, \end{cases} \tag{1}$$

where $\mathcal{X}$ is the input space that contains numerical and categorical dimensions. $X^s \in \mathcal{X}$ (resp. $X^t \in \mathcal{X}$) refers to the input variable of the source domain (resp. target domain), and $Y^s \in \mathcal{Y}$ (resp. $Y^t \in \mathcal{Y}$) refers to the output variable of the source domain (resp. target domain), where $\mathcal{Y}$ is the output space. We also denote by $\mathbb{X}^t = \{x_i \in \mathcal{X} | i = 1, \ldots, n_t\}$, a set of target inputs drawn from $P(X^t)$ with n_t examples, and by $\mathbb{X}^s = \{x_j \in \mathcal{X} | j = 1, \ldots, n_s\}$, a set of source inputs drawn from $P(X^s)$. We study the binary classification problem where $\mathcal{Y} = \{0, 1\}$, and we assume that we are given a pre-trained source model $h_s : \mathcal{X} \to [0, 1]$ corresponding to the source domain optimal Bayes predictor, that is $h_s(x) = P(Y^s{=}1|X^s{=}x)$.

We also assume the existence of an unknown target domain optimal predictor, denoted by $h_t(x) = P(Y^t{=}1|X^t{=}x)$. Accordingly, the second condition of Equation (1) can be reformulated as $h_t(x) = h_s \circ \mathcal{G}(x)$. Notice that $P(Y^s) = P(Y^t)$ is a necessary condition that Equation (1) has a solution, and we can further infer that the following equality holds in this case:

$$P(h_s(X^s)) = P(h_t(X^t)) \,. \tag{2}$$

Following the definition of predictive models, h_s and h_t can be seen respectively as functions of variables X^s and X^t. Equation (2) argues that output distributions of predictive models in two domains should be the same.

Our final proposed DA approach is illustrated in Figure 1. It consists of three steps: output calibration, coordinate-wise adaptation, and feature selection (weakly supervised and unsupervised). The unsupervised feature selection is our primary novelty compared to Zhang et al. [78].

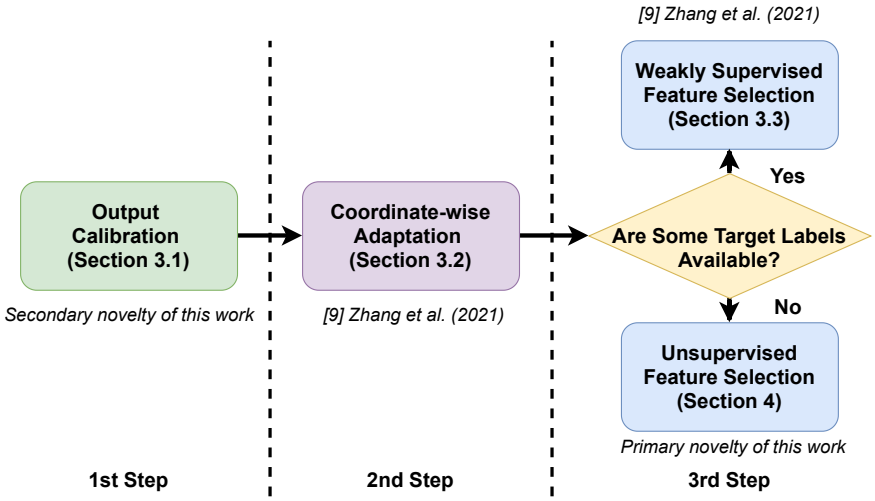

Figure 1: The proposed pipeline of our adaptation method: ***S**tability-based feature selection for **C**oordinate-wise **D**omain **A**daptation* (**SCDA**). Details of each module can be found in the corresponding section.

3.1 Output Calibration

Although it is a common assumption in DA to consider $P(h_s(X^s)) = P(h_t(X^t))$, this condition may be violated in practice. A particular case of violation is the so-called *label shift* [24], where $P(Y^s) \neq P(Y^t)$. Various methods [52, 62, 39] have been proposed to tackle this setting. Note that this paper mainly focuses on the adaptation problem of input spaces, while for completeness, we present in this section how to integrate a simple calibration method [53, 37] to alleviate *label shift* in our proposed *target to source* DA pipeline.

In this paper, we stand in the unsupervised case where neither the target predictor h_t nor the target labels Y^t are given, while the target domain output marginal distribution $P(Y^t)$ is accessible. For example, in a fraud detection system, despite the lack of labels in target domains, one may have the proportion of fraud estimated by experts. Furthermore, we suppose that, for a binary classification problem, if

$$P(Y^s) = P(Y^t)\,, \tag{3}$$

then we have

$$P(h_s(X^s)) = P(h_t(X^t))\,. \tag{4}$$

As input-output pairs (X^s, Y^s) of source domains are given, and target domain output marginal distribution $P(Y^t)$ is also known, one can get Equation (3) by re-weighting source examples by classes. Although re-weighted source data

have no *label shift* compared to target ones, the pre-trained "black-box" model h_s will no longer be optimal in the re-weighted source domain. Thus, in light of the works [53] and [37], we propose calibrating h_s to estimate optimal predictions for examples in the re-weighted source domain. For the simplicity of analysis, we respectively note X^p and Y^p, the input and output variables of the re-weighted source domain. By definition, we have

$$P(Y^p) = P(Y^t) \text{ and } P(X^p|Y^p) = P(X^s|Y^s)\,.$$

Proposition 1 (Source model calibration)**.** Let h_s be the pre-trained optimal binary classifier in the source domain. The optimal predictor $h_p(x) = P(Y^p = 1|X^p = x)$ in the re-weighted source domain is obtained by:

$$h_p(x) = \frac{h_s(x)w(1)}{h_s(x)w(1) + (1 - h_s(x))w(0)}\,, \tag{5}$$

where

$$w(y) = \frac{P(Y^t = y)}{P(Y^s = y)}\,.$$

The details of the proof are given in Appendix. The proposition suggests that the difference between binary output marginal distributions of source and target domains can be mitigated by calibrating outputs of the pre-trained "black-box" model. For the sake of simplicity, hereafter, we consider the source domain is already calibrated, and we use X^s and Y^s instead of X^p and Y^p to express the source domain where data are re-weighted to match the target domain output distribution. Analogously, h_s refers to the calibrated optimal predictive model in the re-weighted domain.

3.2 Optimal Transport for Coordinate-wise Domain Adaptation

The optimal transport problem was first introduced by Monge in the 18th century [44] and further developed by Kantorovich in the mid-20th [26]. Intuitively, the original Monge-Kantorovich problem looks for minimal effort to move masses of dirt to fill a given collection of pits. It is naturally suited for DA problems [11] of tabular data, as it offers a principled method to transform seamlessly numerical and categorical target distributions to source ones. Central to optimal transport methods is the notion of a *cost function* between a source point and a target point, denoted by

$$c : \mathcal{X} \times \mathcal{X} \to \mathbb{R}\,. \tag{6}$$

Moreover, $C \in R^{n_t \times n_s}$ denotes the *cost matrix* between source and target training points such that $C_{i,j} = c(x_i, x_j)$ corresponds to the cost of moving weight from $x_i \in \mathbb{X}^t$ to $x_j \in \mathbb{X}^s$. As discussed at the end of this section, the cost may be defined for categorical and numerical features.

Based on these concepts, we present below the Kantorovich [26] formulation of the multidimensional optimal transport problem in the discrete case.

Definition 1 (Kantorovich's discrete optimal transport problem)**.** The relationship between source and target examples is encoded as a joint probability *coupling matrix* $\gamma \in \mathbb{R}_+^{n_t \times n_s}$, where $\gamma_{i,j}$ corresponds to the *weight* to be *moved* from $x_i \in \mathbb{X}^t$ to $x_j \in \mathbb{X}^s$. The set of admissible coupling matrices is given by

$$\Gamma = \left\{ \gamma \in \mathbb{R}_+^{n_t \times n_s} \;\middle|\; w_i^t = \sum_{j'=1}^{n_s} \gamma_{i,j'} \text{ and } w_j^s = \sum_{i'=1}^{n_t} \gamma_{i',j} \right\},$$

where w_i^t (resp. w_j^s) is the weight of $x_i \in \mathbb{X}^t$ (resp. $x_j \in \mathbb{X}^s$). Typically, we consider that the mass is uniformly distributed among each point, *i.e.*, $w_i^t = 1/n_t$ and $w_j^s = 1/n_s$, but the framework allows reweighing the samples, such that

$$\sum_{i=1}^{n_t} w_i^t = \sum_{j=1}^{n_s} w_j^s = 1\,; \quad w_i^t, w_j^s \geq 0\,.$$

Then, the optimal coupling matrix γ^* is obtained by solving

$$\gamma^* = \underset{\gamma \in \Gamma}{\operatorname{argmin}} \langle C, \gamma \rangle = \underset{\gamma \in \Gamma}{\operatorname{argmin}} \sum_{i=1}^{n_t} \sum_{j=1}^{n_s} C_{i,j} \gamma_{i,j}\,. \tag{7}$$

In turn, the transformation function $\mathcal{G}$ is given by

$$\mathcal{G}(x_i) = \underset{x' \in \mathcal{X}}{\operatorname{argmin}} \sum_{j=1}^{n_s} \gamma_{i,j}^* c(x', x_j)\,. \tag{8}$$

The solution $x' \in \mathcal{X}$ of Equation (8) minimization problem is commonly referred to as the *barycenter mapping* in the optimal transport literature. For unseen target examples x drawn from $P(X^t)$ while $x \notin \mathbb{X}^t$, we project x to its nearest x_i according to $c(x_i, x)$ and then get its source DA using Equation (8).

However, Equation (7) is a linear optimization problem. When $n_s = n_t = n$, the computational complexity is $O(n^3)$ which is not scalable to huge datasets.

Therefore, we restrict the class of transformations $\mathcal{G}$ by considering all features as independent in transfer tasks. Then we propose to use one-dimensional optimal transport individually on each attribute to transform target data to the source domain, which is the so-called *coordinate-wise* adaptation [78]. The transformation $\mathcal{G}$ is decomposed by feature-wise transformations $\mathcal{G}_k$, such that $\mathcal{G} = [\mathcal{G}_1, ..., \mathcal{G}_k, ..., \mathcal{G}_d]$, where d is the number of features of the input space. Each transformation $\mathcal{G}_k$ solves the adaptation problem of the k-th feature by aligning input marginal distributions of this feature between target and source domains, that is, $P(X_k^s) = P(\mathcal{G}_k(X_k^t))$.

Numerical Attribute In the case where the k-th feature is a numerical one, $\mathcal{X}_k = \mathbb{R}$, and the cost function of this dimension is defined as

$$\forall x_i^k, x_{i'}^k \in \mathcal{X}_k\,,\; c_{\text{num}}^p(x_i^k, x_{i'}^k) = |x_i^k - x_{i'}^k|^p\,,$$

where x_i^k and $x_{i'}^k$ stand for the k-th dimension of inputs x_i and $x_{i'}$. Instead of solving $\mathcal{G}_k$ relying on Equation (7) and Equation (8), there is a closed-form solution of the Kantorovich optimization problem [51]:

$$\mathcal{G}_k(x^k) = (F_k^{s\,-1} \circ F_k^t)(x^k)\,, \tag{9}$$

where F_k^s and F_k^t are respectively cumulative distribution functions of $P(X_k^s)$ and $P(X_k^t)$. This solution is also known as increasing arrangement.

Categorical Attribute In contrast, if the k-th feature is categorical, we have $\mathcal{X}_k = D_k$, where $D_k = \{e_1^k, \ldots, e_{n_k}^k\}$ is the (non-ordered) set of values taken by the k-th categorical feature, and n_k is the number of unique values in D_k.

We use a generic strategy that can be applied to any categorical feature by defining the cost in terms of the occurrence frequency [25]:

$$\begin{aligned} &\forall e_l^k, e_r^k \in D_k\,,\ c_{\text{cate}}(e_l^k, e_r^k) = C_{l,r}^k \\ &= \begin{cases} 0 & \text{if } e_l^k = e_r^k\,, \\ 1 - \dfrac{1}{1 + \log(\frac{1}{v_l^k}) \log(\frac{1}{v_r^k})} & \text{otherwise,} \end{cases} \end{aligned} \tag{10}$$

where $v_l^k \in (0, 1]$ (resp. $v_r^k \in (0, 1]$) is the frequency of occurrences of the value e_l^k (resp. e_l^r) for the k-th feature. In Equation (10), we write $C_{l,r}^k$ for the entry of the *cost matrix* $C^k \in \mathbb{R}^{n_k \times n_k}$. Then, we state our optimal transport problem on a categorical feature in terms of the following coupling matrix $\gamma^k \in \mathbb{R}_+^{n_k \times n_k}$ in place of Equation (7):

$$\gamma^k = \underset{\gamma \in \Gamma^k}{\operatorname{argmin}} \left\langle C^k, \gamma \right\rangle = \underset{\gamma \in \Gamma^k}{\operatorname{argmin}} \sum_{l=1}^{n_k} \sum_{r=1}^{n_k} C_{l,r}^k \gamma_{l,r}\,, \tag{11}$$

with

$$\Gamma^k = \left\{ \gamma \in \mathbb{R}_+^{n_k \times n_k} \;\middle|\; \frac{\left|\{i \mid x_i^k = e_l^k\}\right|}{n_t} = \sum_{j=1}^{n_k} \gamma_{l,j} \text{ and } \frac{\left|\{j \mid x_j^k = e_r^k\}\right|}{n_s} = \sum_{i=1}^{n_k} \gamma_{i,r} \right\},$$

where x_i^k (resp. x_j^k) is the k-th dimension of $x_i \in \mathbb{X}^t$ (resp. $x_j \in \mathbb{X}^s$). Therefore, we perform the optimal transport on the n_k categorical values e^k instead of the n_t target (and n_s source) examples. Typically, $n_k \ll n_t$, and the computation is thus less expensive than the original problem. However, unlike numerical features where we can compute a barycenter thanks to Equation (8), the barycenter of categorical features is difficult to define. Consequently, we propose a *stochastic mapping* strategy to tackle this problem. The probability of transforming one value e_l^k to e_r^k is

$$P(\mathcal{G}_k(e_l^k) = e_r^k) = \frac{\gamma_{l,r}^k}{\sum_{j=1}^{n_k} \gamma_{l,j}^k}\,. \tag{12}$$

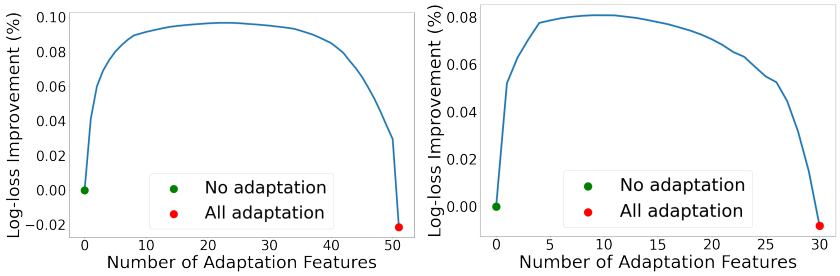

Figure 2: Evolution of log-loss improvements according to the number of adapted features. Left: the Kaggle fraud detection dataset with a neural network pre-trained model. Right: the real fraud detection dataset with a tree-based pre-trained model.

The final prediction score is averaged over each possible transformation weighted by Equation (12).

Therefore, the global computational complexity of the proposed *coordinate-wise* DA is

$$d_{\text{num}} \times \big(n_s \log(n_s) + n_t \log(n_t)\big) + \sum_{k}^{d_{\text{cate}}} (n_k)^3 \,,$$

where d_{num} and d_{cate} respectively refer to the number of numerical and categorical attributes. Although this *coordinate-wise* approach does not take into account correlations between features, it is appealing for the simplicity and the transformations of huge tabular datasets.

3.3 Supervised Feature Selection

In various experiments on different tasks, we have noticed that features contribute differently to DAs. Figure 2 illustrates decreasing percentages of log-loss (log-loss improvement) in a feature selection process. At initialization, no feature is adapted. Then, we transform one more feature to the source domain with the minimal value of log-loss over the target data at each step of the process. We stop when all features are adapted. Note that we use target labels to select the feature to transform at each step only for illustration, whereas they are not accessible in practice. Interestingly, instead of adapting all features, the adaptation of a well-selected subset of features has better performance (larger value of log-loss improvement). Therefore, in the *target to source* DA scenario where a "black-box" source model h_s is available, we aim to seek a subset of features $\alpha \in \mathcal{A}$ to adapt, where $\mathcal{A}$ contains all possible subsets of features of the input space $\mathcal{X}$.

The selected features are adapted one-by-one using *coordinate-wise* optimal transport mapping functions, while other features remain identical without being

excluded from the dataset. Consequently, we can use the source model directly on adapted target data to predict labels. The resulting predictive model of the target domain is expressed by $h_t^\alpha = h_s \circ \mathcal{G}^\alpha$, where $\mathcal{G}^\alpha$ is the transformation function that adapts the feature subset $\alpha \in \mathcal{A}$. We show further in experiments that α generally contains just a few features. Thus, the transformation $\mathcal{G}^\alpha$ is very sparse. Let $\mathcal{G}^*$ be the transformation that verifies Equation (1). Then the optimal target predictor is expressed by $h_t = h_s \circ \mathcal{G}^*$.

In a supervised setting, one tackles this feature selection problem by leveraging labeled data in target domains to find the optimal subset of features that minimizes the expected risk, that is,

$$\alpha^* = \underset{\alpha \in \mathcal{A}}{\operatorname{argmin}} \underset{(x,y)\sim P(X^t,Y^t)}{\mathrm{E}} \left[|h_t^\alpha(x) - y| \right], \tag{13}$$

where $P(X^t, Y^t)$ is the joint distribution of (X^t, Y^t), and the solution α^* is the optimal subset of features to adapt. One may note that $\mathcal{G}^{\alpha^*}$ could be different from $\mathcal{G}^*$, as $\mathcal{G}^{\alpha^*}$ is restricted to the class of *coordinate-wise* transformations, whereas $\mathcal{G}^*$ refers to the optimal transformation among all possible adaptation functions. Nonetheless, $\mathcal{G}^{\alpha^*}$ is appealing for its interpretability, as the selected subset of features α^* reveals the gap between source and target domains.

However, in typical DA problems, $P(X^t, Y^t)$ is unknown; thus, directly minimizing Equation (13) is not feasible. When few labeled target data are available, *i.e.,* in a weakly supervised setting, we proposed [78] to seek the subset of features that minimizes the following term:

$$\hat{\alpha}^* = \underset{\alpha \in \mathcal{A}}{\operatorname{argmin}} \frac{1}{n_q} \sum_{(x,y)\in\mathbb{Q}} \left| h_t^\alpha(x) - y \right|, \tag{14}$$

where $\mathbb{Q} = \{(x_i, y_i) | i = 1, \ldots, n_q\}$ contains n_q labeled target examples, and n_q is very small. Despite the promising performance obtained by weakly-supervised methods, one still needs labeled data in the target domain.

4 Unsupervised Feature Selection Based on Stable Pseudo-Labeling

In this paper, we address a more challenging unsupervised DA setting where target labels, even few labeled examples, are not available ($n_q = 0$). However, the set of target inputs $\mathbb{X}^t$ is given. Intuitively, if one gets an estimator $\hat{h}$ to annotate some specific target examples $x \in \mathbb{X}^t$ approximately, one can solve the feature selection problem by injecting $\hat{h}$ into Equation (14) to replace y. Since $\hat{h}$ does not generalize to new target examples, one cannot directly use it as the target domain predictor. Nevertheless, it can serve as an adequate "anchor" for the unsupervised feature selection process. Such approximate annotations are the so-called pseudo-labels.

One of the most well-known strategies is to estimate target pseudo-labels using predictions of source models directly, assuming that high-confidence predictions

are correct [81, 8, 54]. However, we illustrate further on a toy example (Figure 3) that this approach could be unstable and gives incorrect pseudo-labels in some cases. In contrast, instead of pseudo-labeling target examples with confident predictions, we estimate pseudo-labels of examples with rank-stable predictions under different transformation functions.

4.1 Rank Stability

In this section, we define a notion of *stable inputs* suited for our DA task. Namely, we propose a pseudo-label estimator, and we prove that our method gives pseudo-labels equal predictions of the optimal *coordinate-wise* adaptation function, making it legitimate to be applied to the unsupervised feature selection.

Definition 2 (Stable inputs)**.** A target input example $x_i \in \mathbb{X}^t$ is called stable over $\mathcal{A}$ if its rank of prediction remains unchanged after being adapted by *coordinate-wise* transformations over all different feature subsets from $\mathcal{A}$, that is,

$$\begin{aligned} &\forall x_{i'} \in \mathbb{X}^t \,, x_{i'} \neq x_i \,, \forall \alpha, \beta \in \mathcal{A} \,, \\ &h_t^{\alpha}(x_i) > h_t^{\alpha}(x_{i'}) \Longleftrightarrow h_t^{\beta}(x_i) > h_t^{\beta}(x_{i'}) \,. \end{aligned} \tag{15}$$

Accordingly, we denote by $\mathbb{X}^{\mathcal{A}}$ a set of all such target examples.

Furthermore, since α^* is the optimal subset of features to adapt, we suppose that predictions of $h_t^{\alpha^*}$ and h_t on target domain data have the same distribution, that is,

$$P(h_t^{\alpha^*}(X^t)) = P(h_t(X^t)) \,. \tag{16}$$

Under this mild assumption, the following proposition is verified.

Proposition 2 (Property of Stable Inputs)**.** Given that $\mathcal{A}$ contains the optimal subset of features α^*, we have

$$\forall x \in \mathbb{X}^{\mathcal{A}} \,, \forall \beta \in \mathcal{A} \,, \quad H_s^{-1} \circ H_{\beta}(h_t^{\beta}(x)) = h_t^{\alpha^*}(x) \,, \tag{17}$$

where H_s and H_{β} are respectively cumulative distribution functions of $h_s(X^s)$ and $h_t^{\beta}(X^t)$.

Proof. As ranks of predictions can be naturally expressed by cumulative distribution functions, given Equation (15), and α^*, $\beta \in \mathcal{A}$, we have

$$\forall x \in \mathbb{X}^{\mathcal{A}} \,, H_{\alpha^*}(h_t^{\alpha^*}(x)) = H_{\beta}(h_t^{\beta}(x)) \,, \tag{18}$$

where H_{α^*} refers to the cumulative distribution function of $h_t^{\alpha^*}(X^t)$. According to Equations (2) and (16), we have $H_{\alpha^*} = H_t = H_s$. Analogously, H_t is the cumulative distribution function of $h_t(X^t)$. Replacing H_{α^*} to H_s in Equation (18), we get

$$H_s(h_t^{\alpha^*}(x)) = H_{\beta}(h_t^{\beta}(x)) \,.$$

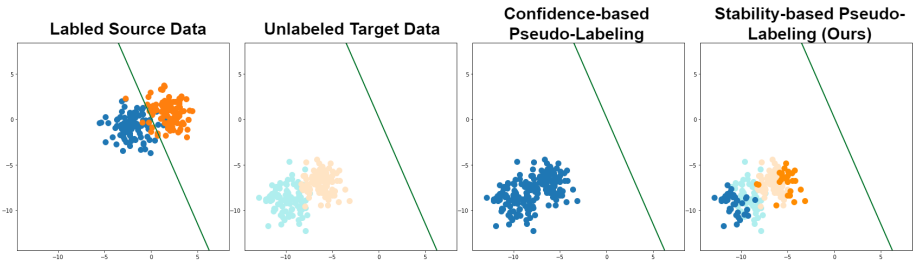

Figure 3: Left: labeled source domain data. Middle left: unlabeled target domain data. Middle right: pseudo-labels given by confidence-based methods. Right: pseudo-labels provided by our proposition over stable target examples. The ground truth of target data is shown in light colors, and pseudo-labels of the target domain are shown in deep colors. The green line in the sub-figures is the pre-trained source domain predictor.

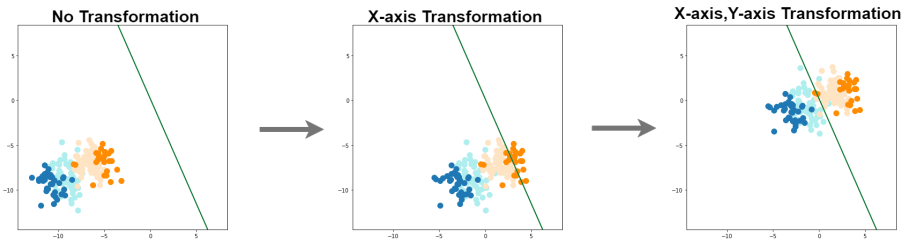

Figure 4: Steps of *coordinate-wise* transformations using stability-based pseudo-labels.

As H_s is invertible, we have

$$h_t^{\alpha^*}(x) = H_s^{-1} \circ H_\beta(h_t^\beta(x))\,,$$

which proves Equation (17). □

Note that $h_t^{\alpha^*}$ is the optimal *coordinate-wise* adaptation function that we expect to get. Therefore, we define the pseudo-label estimator $\hat{h}^\beta(x)$ by the following formula:

Definition 3 (Rank-stable based pseudo-label estimator)**.**

$$\forall x \in \mathbb{X}^{\mathcal{A}}\,, \forall \beta \in \mathcal{A}\,,$$
$$\hat{h}^\beta(x) = H_s^{-1} \circ H_\beta(h_t^\beta(x)) = h_t^{\alpha^*}(x)\,. \tag{19}$$

An example is illustrated in Figure 3, where we compare two different pseudo-labeling techniques on a toy dataset. In this example, we first identify

stable target examples over $\mathcal{A}$, where $\mathcal{A}$ contains all feature subsets of the two-dimensional space. Then we estimate pseudo-labels using $\hat{h}^{\beta}$. Stable examples x with $\hat{h}^{\beta}(x) > 0.5$ are colored as blue and the others as orange. Note that according to Equation (19), the choice of β does not affect the pseudo-labels for all $x \in \mathbb{X}^{\mathcal{A}}$. The pseudo-labeled examples are further used to adapt target data in order to fit the pre-trained source model (Figure 4). We provide details of this process in Section 5. In contrast, confidence-based pseudo-labeling methods (Figure 3 middle right) consider predictions of target examples far from the decision boundary as correct; thus, all examples are pseudo-labeled as blue and provide no information to help DAs. One may note that pseudo-labels given by our method can be close to the decision boundary of the two classes. Indeed, our method is agnostic to the prediction value but relies only on the rank-stability over transformations $\mathcal{G}^{\alpha}, \forall \alpha \in \mathcal{A}$.

Interestingly, we note that our proposition shares some high-level aspects as the multiple knowledge representation (MKR) framework [71], as both methods rely on multiple representations of data to get a robust model. However, MKR aims to leverage representations of different natures, such as hand-crafted representations, deep representations, etc., whereas we adopt the same family of transformations to search for rank consistency of predictions. Moreover, as we propose a fundamentally different DA method compared to *deep adaptation methods*, one future perspective can study the way of applying the MKR framework to combine these two DA methods.

4.2 Relaxation of Rank Stability

The method described in the last subsection is ineffective when the number of examples in $\mathbb{X}^{\mathcal{A}}$ is scarce, as it needs enough *stable* elements to reach a diversity that faithfully expresses the global distribution of X^t. Therefore, we introduce relaxation of Definition 2 to compensate for this scarcity. The relaxation tunes the size of $\mathbb{X}^{\mathcal{A}}$ to reach the right trade-off between the similarity to $\mathbb{X}^t$ and the constraint of Equation (15).

Definition 4 (δ-stable inputs)**.** A target input example $x \in \mathbb{X}^t$ is called δ-stable over $\mathcal{A}$ if

$$\mathcal{B}(x) = \max_{\mu,\nu \in \mathcal{A}} \left(|\hat{h}^{\mu}(x) - \hat{h}^{\nu}(x)| \right) \leq \delta \,. \tag{20}$$

Accordingly, we denote by $\mathbb{X}_{\delta}^{\mathcal{A}}$ an input set that contains all such target examples. By setting $\delta = 0$, one can retrieve Definition 2.

Although one can still use $\hat{h}^{\beta}$ to estimate pseudo-labels for $x \in \mathbb{X}_{\delta}^{\mathcal{A}}$, it is uncertain that Proposition 2 is verified. Intuitively, a larger δ results in a richer $\mathbb{X}_{\delta}^{\mathcal{A}}$ but with a higher risk of violating Proposition 2. In the remainder of this section, we formally analyze the effects of this relaxation over the feature selection process and propose the corresponding unsupervised objective function.

In their seminal DA analysis, [2] proposed to upper bound the expected target domain risk by a sum of three terms: (i) the source domain risk, (ii) the

$\mathcal{H}$-divergence defined as

$$d(P(X^t), P(X^s)) = 2 \sup_{h \in \mathcal{H}} \left| \mathop{\mathrm{E}}_{x \sim P(X^t)} [h(x) \neq 1] - \mathop{\mathrm{E}}_{x \sim P(X^s)} [h(x) \neq 1] \right|$$

to measure the discrepancy between source ($P(X^s)$) and target ($P(X^t)$) input marginal distributions, and (iii) an intrinsic error between true labeling functions of two domains. We denote by

$$\mathcal{E}(\alpha) = \mathop{\mathrm{E}}_{x \sim P(X^t)} \left[|h_t^\alpha(x) - h_t^{\alpha^*}(x)| \right] \tag{21}$$

the target domain risk between a label predictor h_t^α and the optimal one $h_t^{\alpha^*}$. We notice that the drift between $\mathbb{X}_\delta^\mathcal{A}$ and $\mathbb{X}^t$ is known as sample selection bias [22]; thus, we can upper bound $\mathcal{E}(\alpha)$ by considering δ-stable examples $x \in \mathbb{X}_\delta^\mathcal{A}$ as the "source" domain.

Theorem 1. Given a subset of features $\alpha \in \mathcal{A}$, for all $\beta \in \mathcal{A}$, $\delta \in [0, 1]$, the following inequality holds:

$$\mathcal{E}(\alpha) \leq \mathcal{L}(\alpha, \beta, \delta) + \mathcal{D}(\delta)\,, \tag{22}$$

where

$$\mathcal{L}(\alpha, \beta, \delta) = \mathop{\mathrm{E}}_{x \sim P(X_\delta^\mathcal{A})} \left[|h_t^\alpha(x) - \hat{h}^\beta(x)| \right], \tag{23}$$

$$\mathcal{D}(\delta) = \mathop{\mathrm{E}}_{x \sim P(X_\delta^\mathcal{A})} \left[\mathcal{B}(x) \right] + \frac{1}{2} d(P(X^t), P(X_\delta^\mathcal{A}))\,, \tag{24}$$

with $P(X_\delta^\mathcal{A})$ referring to the distribution of δ-stable target inputs.

Proof. According to the Theorem 1 of [2], we have

$$\mathcal{E}(\alpha) \leq \mathop{\mathrm{E}}_{x \sim P(X_\delta^\mathcal{A})} \left[|h_t^\alpha(x) - h_t^{\alpha^*}(x)| \right] + \tfrac{1}{2} d(P(X^t), P(X_\delta^\mathcal{A})) + C.$$

As examples in $\mathbb{X}^t$ and in $\mathbb{X}_\delta^\mathcal{A}$ have the same true labeling function, the constant term $C = 0$. Applying the triangle inequality to the expectation term of the upper bound and we get

$$\mathcal{E}(\alpha) \leq \mathcal{L}(\alpha, \beta, \delta) + \mathop{\mathrm{E}}_{x \sim P(X_\delta^\mathcal{A})} \left[|\hat{h}^\beta(x) - h_t^{\alpha^*}(x)| \right] + \frac{1}{2} d(P(X^t), P(X_\delta^\mathcal{A}))\,.$$

Since $H_{\alpha^*} = H_s$ according to Equation (2) and Equation (16), and relying on Equation (17), we get

$$h_t^{\alpha^*}(x) = H_s^{-1} \circ H_{\alpha^*}(h_t^{\alpha^*}(x)) = \hat{h}^{\alpha^*}(x)\,.$$

As $\beta\,, \alpha^*$ are subsets of $\mathcal{A}$, by replacing $h_t^{\alpha^*}(x)$ with $\hat{h}^{\alpha^*}(x)$ and relying on Equation (20), we have

$$\begin{aligned} & |\hat{h}^\beta(x) - h_t^{\alpha^*}(x)| = |\hat{h}^\beta(x) - \hat{h}^{\alpha^*}(x)| \leq \mathcal{B}(x) \\ \implies & \mathop{\mathrm{E}}_{x \sim P(X_\delta^\mathcal{A})} \left[|\hat{h}^\beta(x) - h_t^{\alpha^*}(x)| \right] \leq \mathop{\mathrm{E}}_{x \sim P(X_\delta^\mathcal{A})} \left[\mathcal{B}(x) \right]. \end{aligned}$$

Theorem 1 is proved. □

In this bound, $\mathcal{L}(\alpha, \beta, \delta)$ refers to the feature selection risk over δ-stable target examples. $\mathcal{D}(\delta)$ encompasses the risk related to the stable inputs relaxation and the discrepancy between $P(X^t)$ and $P(X_\delta^{\mathcal{A}})$. All elements in this upper bound can be computed without target domain labels. Therefore, we define the unsupervised objective function as

$$\tilde{\alpha}^* = \underset{\alpha \in \mathcal{A}}{\operatorname{argmin}} \min_{\beta \in \mathcal{A}} \min_{\delta \in [0,1]} \Big(\mathcal{L}(\alpha, \beta, \delta) + \mathcal{D}(\delta) \Big). \tag{25}$$

Remark. Note that the proposed method is built upon the theoretical bound of the binary DA problem [2]; it is not straightforward to apply to multi-class classifications. Concretely, in a multi-class DA setting, the prediction rank stability requires the orders of predictions in every class remains unchanged, which is too strict. To extend our method to a wider range of applications, we aim to leverage multi-class DA theories [80, 79] and adjust the relaxation function (Equation (20)) to fit their defined multi-class domain discrepancy measures (Definition 3.2 in [80] and Definition 3 in [79]) in our future research.

5 Greedy Algorithm for Feature Selection

Inspired by greedy solvers of classical feature selection methods, we propose the following process to solve Equation (25), and we name our proposed adaptation method: ***S**tability-based feature selection for **C**oordinate-wise **D**omain **A**daptation* (**SCDA**).

5.1 Optimization Process

Set the value of δ Experimental results show that the optimal δ that minimizes the sum of $\mathcal{L}(\alpha, \delta, \beta) + \mathcal{D}(\delta)$ is close to the minimizer of $\mathcal{D}(\delta)$. Therefore, we can rely first on $\mathcal{D}(\delta)$ to estimate the optimal value of δ and then find the couple (α, β) that minimizes $\mathcal{L}(\alpha, \beta, \delta)$. This approach reduces the complexity by simplifying the combination problem of triplets to the combination problem of couples. In practice, we use a grid search algorithm to discretize the value space of δ and estimate empirically $\mathcal{H}$-divergence by training a classifier to distinguish examples between $\mathbb{X}^t$ and $\mathbb{X}_\delta^{\mathcal{A}}$.

Find the optimal subset of features Another issue that we face is the high cardinality of $\mathcal{A}$. As $\mathcal{A}$ contains all possible combinations of subsets of features, and the number of subsets of features grows exponentially with the dimensionality of input data, directly using all possible combinations is sometimes not feasible. A similar problem also exists in the supervised feature selection scenario. We use a greedy search algorithm to tackle this issue. As shown in the forthcoming experiments, our method gives encouraging results in practice. Namely, we let $\mathcal{A}_i$ refer to a subset of $\mathcal{A}$, where i is an index of the greedy search step. As shown in Algorithm 1, no feature is adapted at initialization (steps 1-5). $\mathcal{A}_0$ contains an empty feature subset and all singleton feature sets. We start by

minimizing $\mathcal{D}(\delta)$ to find and set the optimal value of δ (step 5). The variable $Count$ at the step 8 is a dictionary with the structure $\{key : value\}$. We use a bootstrap technique (steps 9-12) at each iteration of the greedy search to get the temporally optimal $\tilde{\alpha}_{i+1}$ (step 13). Then we update $\mathcal{A}_{i+1}$ and continue the process until $\tilde{\alpha}_{i+1}$ remains unchanged or more than one-half of bootstrap datasets are not in accordance with the optimal feature subset.

Algorithm 1 Greedy Search Algorithm

1: Initialize $i = 0$.
2: Initialize $\tilde{\alpha}_0 = \varnothing$.
3: Initialize $\mathcal{A}_0 = \{\varnothing\} \cup \{\{j\} | \forall j \in \mathcal{A}\}$.
4: Initialize $v_0 = 1$.
5: Initialize $\delta = \text{argmin}_\delta \mathcal{D}(\delta)$.
6: **repeat**
7: Get $X_\delta^{\mathcal{A}_i}$ using Definition 4 on $\mathcal{A}_i$ and fixed δ.
8: Initialize $Count[\alpha] = 0$ for all $\alpha \in \mathcal{A}_i$.
9: **for** X^B **in** bootstraps of $X_\delta^{\mathcal{A}_i}$ **do**
10: $(\alpha, \beta) =$ minimizer of $\mathcal{L}(\alpha, \beta, \delta)$ on P_{X^B} and fixed δ.
11: $Count[\alpha] = Count[\alpha]+1$.
12: **end for**
13: $\tilde{\alpha}_{i+1} = \text{argmax}_\alpha Count[\alpha]$.
14: $\mathcal{A}_{i+1} = \{\tilde{\alpha}_{i+1}\} \cup \{\tilde{\alpha}_{i+1} \cup \{j\} | \forall j \in \mathcal{A} / \tilde{\alpha}_{i+1}\}$.
15: $v_{i+1} = Count[\tilde{\alpha}_{i+1}] / \sum_\alpha Count[\alpha]$.
16: **until** $\tilde{\alpha}_{i+1}$ unchanged or $v_{i+1} < 0.5$; $i = i + 1$.
17: **return:** $\tilde{\alpha}_i$

Complexity of the greedy algorithm The computational complexity of the greedy feature selection for a target dataset with n_s examples and d dimensions is $O(n_s d^2)$. Although the feature selection process seems not scalable over high-dimensional data, we show further in experiments that only very few features are selected for DA. Therefore, the number of operations is far less than $O(n_s d^2)$ in practice. Moreover, the minimization problem (step 10 in Algorithm 1) consists of finding the optimal couple (α, β) from $\mathcal{A}_i \times \mathcal{A}_i$. One can accelerate this optimization problem by partitioning $\mathcal{A}_i \times \mathcal{A}_i$ into several smaller search spaces and parallelizing the searching process.

6 Experiments

In this section, we evaluate the performances of our adaptation method SCDA on 3 different datasets and 2 types of models: Gradient Boosting Decision Tree (GBDT) and neural networks (NN). We use respectively LightGBM [27] and PyTorch [49] packages in Python to implement these models. The source code of experiments is available on Github: `www.github.com/marrvolo/SCDA`.

6.1 Setup Overview

Kaggle Fraud Detection Dataset[1] The dataset contains payment transactions issued from mobile devices and desktop devices, and one aims to predict if an online transaction is fraudulent or not. The raw data dimension is over 400, while most features contain missing values and some are not discriminative. We discard features with more than 1% of missing values and all transactions containing missing values. To discard label-irrelevant features, we first train a predictive model in a supervised setting and predict on test data where one feature's values are randomly shuffled. The feature is considered label-irrelevant if the prediction performance remains nearly the same compared to the not-shuffled one. After preprocessing, the dataset used in experiments has around 400,000 examples with 43 numerical features and 8 categorical ones. We consider the mobile device as the source domain and the desktop device as the target domain in our DA scenario. The proportions of fraud in each domain are respectively 10% and 7%. We correct the *label shift* relying on Proposition 1. We perform a 4-fold validation by dividing mobile and desktop transactions into 4 parts and denoting each part respectively by M-1 to M-4 (mobile device) and D-1 to D-4 (desktop device). Following this setting, the *target to source* DA transforms data from D-i to M-i.

Real Fraud Detection Dataset[2] This dataset consists of real anonymous clients' transactions from July 2018 to September 2018 of two geographical domains: Belgium and Germany. Both datasets have 23 numerical attributes and 7 categorical ones. All features are generated by experts in payment and are thus discriminative. The number of examples in the Belgian dataset is over 30 million and around 15 million in the German dataset. The proportions of fraud are respectively 0.3% and 0.5% in the two countries. We correct the *label shift* relying on Proposition 1. Note that classes of labels are highly unbalanced in Kaggle and real fraud detection datasets, thus completing DA tasks. Moreover, in the real fraud detection task, the data distribution naturally "drifts" as time goes by. For example, the Belgian data distribution in July is not the same as the one in August. Consequently, we build 3 source (target) domains where each month of Belgian (German) data is considered one domain. We denote by Bel-1 to Bel-3 the source domains and by Ger-1 to Ger-3 the target domains. Following this setting, the *target to source* DA transforms data from Ger-i to Bel-i. Due to confidential reasons, this dataset is not shared.

Although we evaluate our methods on two fraud detection datasets, the drifts between source and target domains of these two datasets are different. In the Kaggle fraud detection task, the drift comes from device change. In contrast, source and target distributions differ as geographical localization (users' payment habits) and time change in the real fraud detection task. Hence, they are entirely two different DA tasks.

[1] `www.kaggle.com/c/ieee-fraud-detection`

[2] This private transaction dataset is provided by an IT company.

Amazon Reviews Dataset The dataset contains reviews of buyers on the Amazon website across different categories of products [3]. Each review is a small paragraph of texts, transformed into bags-of-words representation and labeled as positive or negative. Note that the sentiment classification model trained using supervised learning to predict buyers' points of view for one category does not directly generalize to another. Following the setting of Chen et al. [9], we consider 4 domains: Books (B), DVDs (D), Electronics (E), and Kitchen appliances (K). Each domain has 2,000 training examples and around 4,000 test examples with perfectly balanced labels. We keep the most frequent 400 words dimensions and generate features from bags-of-words representations using mSDA unsupervised auto-encoder [9] with 5 layers. Instead of stacking all hidden dimensions as Chen et al. [9] and Ganin et al. [18], we take only the representation of the last layer. Different from the aforementioned two fraud detection datasets, the features of the Amazon reviews dataset may not have explicit meaning that can be easily interpreted.

Other General Setup Details We pre-train source domain predictive models using supervised learning with 10 different random states and keep the one that achieves the best performance on source domain test datasets. One NN model and one GBDT model are built for each source domain of different tasks following this process. An embedding layer is applied for NN models to transform categorical features into numerical representations, followed by three fully connected hidden layers. For GBDT models, we use raw categorical data without transformation. We compare our proposed method (SCDA) with *deep adaptation methods*: DAN [40], DANN [18], MCD [55], and the state-of-the-art DA method on image datasets HDA+ToAlign [12, 70], as well as *classical adaptation methods*: CORAL [61], OTLin with a linear kernel [50], and CDA [78] that uses *coordinate-wise* transformations to adapt all features without a feature selection process.

Remark. We have also evaluated the method proposed by [67]. However, its performances are significantly worse than all other deep adaptation methods reported in the experiments. Therefore, we did not include this method in the experiments. Our intuition is that the method optimizes several modules of neural networks individually, which is hard to converge on our highly imbalanced datasets.

As described in Section 3.2, SCDA selects features based on *coordinate-wise* transformations. Therefore, we use the POT [16] package to compute such optimal transport mappings. We chose to compare with CORAL and OTLin methods as they perform DAs without modifying the input space of data. As a result, we can extend such methods to address *target to source* DAs and leverage pre-trained GBDT models and NN models to predict target labels. However, they do not adapt categorical features. In contrast, *deep adaptation methods* can transform categorical attributes, whereas they do not satisfy the *target to source* DA setting. *Deep adaptation methods* transform source and target domain data into a latent space and require training a predictive model using source labels

during adaptation processes.

Our SCDA approach is *feature-type free* and *hyper-parameter free*, such that no tuning process is required. *Deep adaptation methods* require finding the optimal weight of the adversarial (regularization) term and the learning rate. To select the optimal hyper-parameter for *deep adaptation methods*, we use a grid search process during the training and take the hyper-parameter that minimizes the classification error on test datasets of source domains. We seek hyper-parameter in the set of values $\{0.01, 0.05, 0.1\}$ for DANN and DAN methods of the Amazon reviews datasets. For the Kaggle fraud detection dataset, the set of values that we used to search the hyper-parameter is $\{0.005, 0.01, 0.1\}$ for DAN models and $\{0.05, 0.1, 0.5\}$ for DANN models. As for MCD and HDA+ToAlign models, the Amazon review tasks seek the learning rate among $\{0.0001, 0.0005, 0.001, 0.005\}$, and the Kaggle fraud detection tasks seek the learning rate among $\{0.0005, 0.0007, 0.001\}$.

6.2 Adaptation Performance

We consider the performance of using directly pre-trained source models on target test datasets as baselines. Since we expect predictive models to be well-calibrated, we use the decreasing percentage of log-loss compared to the baseline as our evaluation metric. A positive value of metric means the adaptation method improves the performance of predicting target domain labels, whereas a negative value refers to the negative transfer. Besides, we also report performances in terms of *area under the precision-recall curve* (PR_AUC) for fraud detection tasks and in terms of accuracy for the Amazon review tasks. All experiments are repeated 10 times with different random states, and standard deviations are reported to illustrate the stability of the methods.

Kaggle Fraud Detection Dataset Table 2a and Table 2c present performances of *classical adaptation methods* and our propositions using GBDT models. SUPERVISED stands for the results of supervised greedy feature selection. We estimate transformation functions of CORAL and CDA using all training input examples of source and target domains. In contrast, SCDA is trained with only 20% of input examples to accelerate the process of greedy search. OTLin does not address the problem of huge datasets; thus, we draw 2,000 input examples from each domain to compute the *target to source* mapping, and we present this result as OTLin(2K). Following the same setting as OTLin(2K), we refer to the performance of SCDA on 2,000 examples as SCDA(2K). As our proposition estimates the transformations one dimension by one dimension, it can be trained using only a few input examples. Moreover, as CORAL and OTLin do not adapt categorical features, only numerical features are transformed by these two methods, while other methods adapt all features. On average and for each adaptation task, our propositions SCDA and SCDA(2K) achieve the best performance among all adaptation methods. Interestingly, SCDA(2K) achieves better performances than adaptation methods trained using more input examples. One may notice that CORAL and OTLin have a negative transfer using GBDT

(a) The log-loss improvement (%) of GBDT models.

Method	D-1 to M-1	D-2 to M-2	D-3 to M-3	D-4 to M-4	Avg
SUPERVISED	13.41±0.12	15.30±0.36	10.76±0.24	11.46±0.29	12.73
CORAL	-13.76±0.47	-3.25±0.45	-14.06±0.31	-33.30±0.83	-16.09
OTLin(2K)	-11.66±3.60	-0.81±1.82	-14.19±2.29	-17.41±2.93	-11.02
CDA	9.37±0.20	12.36±0.24	6.71±0.19	7.61±0.20	9.01
SCDA	12.69±0.16	14.35±0.08	10.00±0.24	10.19±0.26	11.81
SCDA(2K)	**12.82±0.26**	**14.72±0.14**	**10.67±0.23**	**10.93±0.25**	**12.29**

(b) The log-loss improvement (%) of NN models.

Method	D-1 to M-1	D-2 to M-2	D-3 to M-3	D-4 to M-4	Avg
SUPERVISED	13.60±0.12	12.61±0.22	21.38±0.18	17.65±0.56	16.31
DANN	2.65±7.41	0.09±3.83	7.15±3.20	4.40±2.89	3.57
DAN	7.36±5.08	-1.27±5.36	6.99±4.90	4.18±5.39	4.31
MCD	9.21±2.73	4.71±3.64	9.29±2.84	9.84±1.80	8.26
HDA+ToAlign	4.35±7.25	-0.82±6.67	3.17±6.97	2.42±6.51	2.28
CORAL	3.69±0.18	-5.18±0.27	-0.99±0.19	3.00±0.20	0.13
OTLin(2K)	6.33±2.18	-1.67±2.25	1.65±3.11	8.53±1.37	3.71
CDA	8.37±0.29	5.14±0.20	13.55±0.22	12.36±0.32	9.86
SCDA	**11.84±0.25**	**8.85±0.87**	**19.56±0.46**	14.60±0.63	**13.71**
SCDA(2K)	11.40±1.33	6.88±0.85	18.95±0.41	**15.18±0.53**	13.10

(c) The PR_AUC improvement (%) of GBDT models.

Method	D-1 to M-1	D-2 to M-2	D-3 to M-3	D-4 to M-4	Avg
SUPERVISED	2.53±0.25	4.95±0.60	3.34±0.35	2.92±0.22	3.44
CORAL	-8.98±0.37	-9.91±0.38	-13.13±0.25	-17.96±0.37	-12.50
OTLin	-14.62±1.81	-10.37±1.67	-17.23±2.71	-13.38±2.84	-13.90
CDA	-0.43±0.24	2.37±0.26	-1.45±0.25	-0.91±0.28	-0.10
SCDA	**2.15±0.08**	4.25±0.13	3.02±0.15	2.55±0.17	2.99
SCDA(2K)	2.01±0.32	**4.38±0.23**	**3.34±0.30**	**3.04±0.21**	**3.19**

(d) The PR_AUC improvement (%) of NN models.

Method	D-1 to M-1	D-2 to M-2	D-3 to M-3	D-4 to M-4	Avg
SUPERVISED	4.14±0.34	3.16±0.24	4.73±0.14	4.79±0.34	4.21
DANN	-3.40±5.88	-4.67±3.53	-6.02±4.40	-4.08±3.68	-4.54
DAN	-1.52±5.66	-5.22±4.49	-5.10±3.71	-4.33±5.77	-4.04
MCD	1.76±3.09	-0.99±2.26	-2.84±2.94	-1.03±2.10	-0.77
HDA+ToAlign	0.18±6.87	-2.34±6.31	-6.61±7.29	-4.47±7.19	-3.31
CORAL	-5.72±0.17	-12.97±0.24	-17.14±0.33	-14.04±0.20	-12.47
OTLin	-5.34±3.15	-12.85±3.15	-17.45±4.78	-8.22±3.21	-10.96
CDA	0.70±0.16	-1.14±0.20	-0.24±0.27	2.04±0.27	0.34
SCDA	**2.08±0.35**	**0.38±0.62**	**3.67±0.30**	2.50±0.35	**2.16**
SCDA(2K)	1.72±1.74	-0.15±0.58	3.23±0.55	**3.27±0.85**	2.02

Table 2: Adaptation performances of Kaggle fraud detection tasks.

(a) The maximum log-loss improvement (%) of NN models.

Method	D-1 to M-1	D-2 to M-2	D-3 to M-3	D-4 to M-4	Avg
DANN	7.97	7.21	12.69	8.81	9.17
DAN	**14.25**	6.86	11.83	9.59	10.64
MCD	12.74	**10.51**	13.41	12.76	12.35
HDA+ToAlign	12.97	7.47	13.68	10.78	11.22
SCDA	12.30	10.44	**20.09**	**15.54**	**14.59**

(b) The maximum PR_AUC improvement (%) of NN models.

Method	D-1 to M-1	D-2 to M-2	D-3 to M-3	D-4 to M-4	Avg
DANN	3.18	0.04	0.17	0.44	0.96
DAN	5.23	1.26	-0.13	1.93	2.07
MCD	**6.53**	**3.58**	1.42	2.52	3.51
HDA+ToAlign	6.32	3.13	2.02	**3.09**	**3.64**
SCDA	2.82	1.67	**4.06**	3.04	2.90

Table 3: The maximum improvement of adaptation methods with different random states on the Kaggle fraud detection tasks.

Method	D-1 to M-1	D-2 to M-2	D-3 to M-3	D-4 to M-4	Avg
SCDA GBDT	14.9±4.8	15.3±3.0	18.9±5.4	16.9±2.9	16.5
SCDA(2K) GBDT	8.0±3.2	8.1±2.1	6.3±1.1	7.1±1.6	7.3
SCDA NN	12.2±3.1	9.9±3.1	12.6±2.6	11.3±4.1	11.5
SCDA(2K) NN	9.9±1.8	3.4±2.1	4.5±1.5	4.9±1.5	5.6

Table 4: Number of adapted features of GBDT and NN models.

models. We explain this observation by the fact that they adapt only numerical features, which may be harmful to GBDT models.

Regarding NN models, similar conclusions can be drawn from Table 2b and Table 2d. *Deep adaptation methods* use all input examples and map categorical features to numerical spaces by an embedding layer so that categorical values can be transformed like numerical ones. On average, DANN, DAN, MCD, and HDA+ToAlign methods improve the performance compared to no-adaptation by respectively 3%, 4%, 8% and 2% in terms of log-loss improvements. In contrast, they perform negative transfers in terms of PR_AUC and have high standard deviations for every adaptation task. Alternatively, our proposition outperforms all adaptation methods and is robust in performance. Experimental results support our intuition that *deep adaptation methods* are complicated to train in an unsupervised setting. Moreover, note that *classical adaptation methods* like CORAL and OTLin perform differently in GBDT and NN models in terms of log-loss improvements, whereas our propositions are totally model-independent. As we work with unbalanced datasets, performance improvements in terms of PR_AUC are generally less significant than log-loss.

The adaptation performances in Table 2b and Table 2d appear to show that *deep adaptation methods* do not improve the Kaggle fraud detection tasks in most cases. However, if we focus only on the best occurrence of different

random states (Table 3), all *deep adaptation methods* significantly increase the prediction performances. Indeed, the studied *deep adaptation methods* require a tedious hyper-parameter searching process. Even the value of the random state has a non-negligible impact on their performances. Nevertheless, finding the optimal hyper-parameters (random state) in an unsupervised DA setting is not straightforward. Such instability to hyper-parameters hinders the generalization of *deep adaptation methods* to our DA tasks.

Table 4 reports respectively the number of adapted features selected by our methods with GBDT and NN pre-trained models. Note that in the setting of 2,000 input examples, we adapt fewer features in general. Both the sparsity of selected features and the orders of their selections can help business experts explain customers' different payment habits in two domains. Note that methods like CDA improve prediction performances as well; however, no insights on drifts between domains are provided.

Real Fraud Detection Dataset In this task, we follow a similar setting as Kaggle fraud detection experiments, where SCDA is trained this time using 1% of input data to accelerate the feature selection process. Table 5a and Table 5c reveal performances with GBDT pre-trained model in terms of log-loss and PR_AUC improvements, and Table 5b and Table 5d reveal performances with NN pre-trained models.

On average, the SCDA method outperforms other adaptation methods in both metrics when using GBDT models to predict target labels. Although trained with very few input examples, SCDA(2K) is the second-best on average in terms of log-loss improvements. Regarding NN models, SCDA outperforms other methods in terms of PR_AUC. It achieves the best performance in terms of log-loss improvements when adapting from Ger-1 to Bel-1 and has comparable results to CDA (adapting all features) when transforming Ger-3 to Bel-3. However, for the adaptation task Ger-2 to Bel-2, different conclusions can be drawn from two metrics. In terms of PR_AUC, SCDA outperforms all other methods on this task, whereas it decreases the performance compared to CDA in terms of log-loss. Our proposition minimizes the absolute difference between estimated predictions and the optimal prediction values by leveraging on the work of Ben-David et al. [2], which is directly related to log-loss. However, the metric PR_AUC only takes into account orders between predictions. Consequently, relative performances in terms of log-loss and PR_AUC improvements may have different results. In both GBDT models and NN models, OTLin does not improve performances compared to no-adaptation, which is probably because only a few input examples are used to estimate transformation functions.

Deep adaptation methods can achieve promising results in some tasks, such as the adaptation task Ger-3 to Bel-3 of DANN and the adaptation task Ger-1 to Bel-1 of MCD. However, the optimal hyper-parameter is complicated to find without label information. One may note that DANN suffers in the adaptation task Ger-2 to Bel-2 and fails to converge. Alternatively, our adaptation method is parameter-free and requires no retraining of predictive models; thus, we do

(a) The log-loss improvement (%) of GBDT models.

Method	Ger-1 to Bel-1	Ger-2 to Bel-2	Ger-3 to Bel-3	Avg
SUPERVISED	6.81±0.26	14.52±0.12	10.87±0.23	10.73
CORAL	0.73±0.01	4.13±0.01	-0.91±0.01	1.32
OTLin(2K)	-15.09±3.24	-13.07±2.35	-8.76±2.21	-12.31
CDA	3.08±0.05	9.52±0.04	5.37±0.05	5.99
SCDA	**4.13±0.22**	**12.71±0.36**	**5.42±0.99**	**7.42**
SCDA(2K)	3.63±0.82	11.81±2.42	4.21±1.07	6.55

(b) The log-loss improvement (%) of NN models.

Method	Ger-1 to Bel-1	Ger-2 to Bel-2	Ger-3 to Bel-3	Avg
SUPERVISED	17.41±0.21	12.10±0.24	8.18±0.86	12.56
DANN	13.90±1.67	-405.76±154.74	**9.14±1.72**	-127.58
DAN	13.52±1.64	-1.53±3.81	-4.45±5.38	2.52
MCD	16.65±2.49	5.80±3.98	-3.82±6.74	6.21
HDA+ToAlign	11.70±1.69	0.30±1.75	3.71±3.51	5.24
CORAL	-17.77±0.02	-1.91±0.01	3.15±0.01	-5.51
OTLin(2K)	-14.96±1.38	-9.12±1.43	-9.23±1.47	-11.10
CDA	14.57±0.06	**9.58±0.09**	5.83±0.07	**9.99**
SCDA	**17.13±0.16**	4.63±2.30	5.61±0.34	9.12
SCDA(2K)	14.06±7.28	4.28±3.48	2.64±0.94	6.99

(c) The PR_AUC improvement (%) of GBDT models.

Method	Ger-1 to Bel-1	Ger-2 to Bel-2	Ger-3 to Bel-3	Avg
SUPERVISED	6.31±0.63	20.93±2.01	6.08±0.85	11.10
CORAL	-8.75±0.04	-6.97±0.03	-19.37±0.05	-11.70
OTLin(2K)	-50.57±10.44	-40.04±5.41	-44.33±5.39	-44.98
CDA	5.30±0.25	**14.95±0.36**	-2.11±0.18	6.05
SCDA	**5.47±0.87**	13.24±1.91	**0.76±0.77**	**6.49**
SCDA(2K)	3.77±0.77	12.44±6.37	0.65±2.74	5.62

(d) The PR_AUC improvement (%) of NN models.

Method	Ger-1 to Bel-1	Ger-2 to Bel-2	Ger-3 to Bel-3	Avg
SUPERVISED	26.49±0.75	2.26±1.26	7.13±0.69	11.96
DANN	-3.33±6.30	-62.05±37.60	**8.92±3.32**	-18.82
DAN	6.07±8.38	-3.40±6.84	1.32±4.58	1.33
MCD	19.73±8.15	-2.05±5.89	8.01±4.61	8.57
HDA+ToAlign	8.94±5.52	-5.40±7.81	3.72±5.71	2.42
CORAL	-7.44±0.02	-8.50±0.04	-5.57±0.04	-7.17
OTLin(2K)	-41.69±5.15	-31.15±3.36	-36.20±2.99	-36.35
CDA	19.19±0.19	1.58±0.27	1.16±0.19	7.31
SCDA	**24.38±0.53**	**4.09±0.70**	1.96±1.63	**10.15**
SCDA(2K)	19.44±10.39	1.00±3.19	-0.95±3.35	6.50

Table 5: Adaptation performances of real fraud detection tasks.

Method	Ger-1 to Bel-1	Ger-2 to Bel-2	Ger-3 to Bel-3	Avg
SCDA GBDT	8.7±3.1	7.7±0.7	7.7±1.0	8.0
SCDA(2K) GBDT	3.7±2.7	5.1±3.1	6.4±2.3	5.0
SCDA NN	5.7±1.8	4.5±1.4	8.0±1.3	6.0
SCDA(2K) NN	4.5±2.9	3.3±1.8	4.5±2.9	4.1

Table 6: Number of adapted features of GBDT and NN models.

not need a time-consuming manual tuning procedure. *Classical adaptation methods* like CORAL and OTLin do not appear to have an adequate adaptation performance since they transform only numerical features and do not address the adaptation problem of extremely unbalanced classes.

Table 6 reports the number of adapted features of each task. For the pre-trained GBDT models, SCDA selects 8 features on average, and SCDA(2K) selects 5 features. Regarding NN models, SCDA selects 6 features, and SCDA(2K) selects 4 features. By adapting very few features, we can achieve comparable or better performances than methods that adapt all features.

Amazon Reviews Dataset As introduced in the setup of experiments, different from fraud detection datasets, features of Amazon reviews datasets are generated using a particular neural network: auto-encoder. As a result, individual features may not have interpretable meanings. Table 7a to Table 7d provide results of Amazon reviews datasets using GBDT and NN models in log-loss and accuracy. Adaptation results appear to show that SCDA does not improve performances compared to the all adaptation method (CDA). However, as shown in Table 7e, SCDA adapts only 5.4 features on average among 400 to achieve these results for GBDT models. Regarding NN models, SCDA transforms 10.2 features on averages.

The forward feature selection process appears to stop at a very early step and seems to be stuck at local minima. We explain this phenomenon by the fact that features generated by neural networks are highly correlated (see Figure 5). The greedy algorithm that considers at each step only one feature may not be able to identify all features that contribute to DAs in this case. However, in a classical tabular dataset, since all features are generated manually, and redundant features are removed, it is less common to have highly correlated features like the ones generated by neural networks.

Nevertheless, by adapting on average 5.4 features for GBDT models and 10.2 features for NN models, our unsupervised adaptation method SCDA achieves the second-best among all methods in Table 7c, Table 7a, and Table 7b.

Compared to the transport theory method OTLin, which adopts a multi-dimensional Euclidean distance to transform all features at once, our proposition shows better results with an ability to handle a high number of dimensions through a one-by-one feature adaptation.

(a) The log-loss Improvement (%) of GBDT models.

Method	D to B	E to B	K to B	B to D	E to D	K to D	B to E	D to E	K to E	B to K	D to K	E to K	Avg
SUP	0.97±0.19	3.68±0.02	5.63±0.02	1.73±0.07	8.83±0.02	11.97±0.04	2.40±0.05	1.37±0.04	1.98±0.03	3.58±0.05	2.65±0.01	2.67±0.05	3.96
CORAL	-0.80±0.00	-2.36±0.00	-0.76±0.00	-0.14±0.00	2.02±0.00	5.78±0.00	-2.28±0.00	-2.65±0.00	0.26±0.00	1.61±0.00	-0.47±0.00	**2.32±0.00**	0.21
OTLin	-4.33±0.00	-3.99±0.00	-3.76±0.00	-4.41±0.00	-1.00±0.00	0.69±0.00	-5.87±0.00	-5.66±0.00	-5.77±0.00	-2.62±0.00	-4.25±0.00	-1.86±0.00	-3.57
CDA	0.29±0.02	**0.60±0.01**	2.26±0.02	**1.06±0.04**	**5.09±0.03**	**8.01±0.03**	**0.29±0.01**	**0.02±0.02**	**1.69±0.02**	**2.88±0.04**	**1.07±0.02**	2.23±0.01	**2.13**
SCDA	**0.39±0.03**	0.55±0.27	**2.46±0.57**	0.87±0.21	2.79±0.95	7.37±2.29	-0.32±0.07	-0.39±0.15	1.50±0.11	2.15±0.39	-0.08±0.14	1.95±0.02	1.60

(b) The log-loss Improvement (%) of NN models.

Method	D to B	E to B	K to B	B to D	E to D	K to D	B to E	D to E	K to E	B to K	D to K	E to K	Avg
SUP	0.96±0.01	12.31±0.01	18.91±0.00	0.17±0.01	5.74±0.00	9.50±0.00	7.88±0.02	3.70±0.01	5.46±0.00	3.97±0.03	4.45±0.05	1.27±0.00	6.19
DANN	-5.02±1.15	6.75±2.32	11.62±2.55	-2.16±0.77	0.07±1.44	1.04±1.88	-1.98±4.25	-1.23±2.44	-0.59±1.26	0.88±0.87	1.44±0.94	-3.96±1.13	0.57
DAN	-1.45±0.30	**10.63±0.59**	10.81±1.03	-1.19±0.46	4.24±0.50	7.27±0.50	**5.51±1.42**	1.51±0.74	-1.07±3.50	-1.51±1.11	-3.02±0.95	-1.08±1.22	2.55
MCD	-3.20±2.66	7.65±1.94	10.72±3.65	-0.72±0.55	0.03±2.73	-0.40±4.32	-5.35±4.48	-2.90±2.48	3.21±0.85	1.19±1.39	1.00±2.36	-2.41±2.25	0.42
HDA+ToAlign	-2.56±1.12	2.21±3.99	5.37±4.64	-1.99±1.96	-3.25±5.19	-1.86±7.13	3.02±3.34	1.18±2.01	1.01±3.63	2.53±2.39	1.99±1.45	-3.18±2.50	0.37
CORAL	0.31±0.00	7.88±0.00	14.54±0.00	-0.68±0.00	2.65±0.00	6.10±0.00	-1.15±0.00	-2.97±0.00	3.79±0.00	-3.06±0.00	-2.76±0.00	-1.75±0.00	1.91
OTLin	-6.30±0.00	5.74±0.00	10.49±0.00	-4.64±0.00	0.69±0.00	3.12±0.00	-4.45±3.77	-2.23±2.46	1.71±0.98	1.34±0.76	2.08±0.58	-2.41±2.25	0.84
CDA	**0.35±0.01**	9.77±0.00	**16.68±0.00**	-0.65±0.00	**5.24±0.00**	**8.94±0.00**	5.42±0.00	**2.25±0.00**	**4.90±0.00**	**1.58±0.00**	**2.44±0.01**	-0.65±0.00	**4.69**
SCDA	-0.55±0.06	7.85±0.56	14.23±0.22	**-0.12±0.04**	3.04±0.20	6.38±0.02	3.23±0.51	-0.68±0.15	4.69±0.11	-0.78±0.41	-1.33±1.38	**-0.10±0.07**	2.99

(c) The Accuracy Improvement (%) of GBDT models.

Method	D to B	E to B	K to B	B to D	E to D	K to D	B to E	D to E	K to E	B to K	D to K	E to K	Avg
SUP	0.97±0.37	0.68±0.02	1.78±0.03	1.54±0.11	6.74±0.03	10.66±0.09	1.26±0.13	0.51±0.06	0.81±0.03	2.17±0.06	1.87±0.05	1.21±0.03	2.52
CORAL	-1.46±0.00	-3.82±0.00	-1.10±0.00	**1.51±0.00**	3.22±0.00	7.08±0.00	-0.26±0.00	-1.11±0.00	-0.11±0.00	2.21±0.00	0.64±0.00	**1.33±0.00**	0.68
OTLin	-2.52±0.00	-3.27±0.00	-3.00±0.00	-2.15±0.00	1.02±0.00	4.81±0.00	-2.03±0.00	-1.83±0.00	-2.45±0.00	1.27±0.00	-2.04±0.00	0.41±0.00	-0.98
CDA	**-0.13±0.06**	-0.03±0.05	0.94±0.03	1.03±0.09	**5.84±0.06**	**8.57±0.05**	0.25±0.04	-0.19±0.08	0.37±0.05	**2.54±0.03**	0.57±0.04	0.94±0.02	**1.73**
SCDA	-0.28±0.00	**0.37±0.27**	**0.99±0.18**	-0.06±0.36	2.06±1.06	7.72±2.58	**0.32±0.08**	**0.27±0.14**	**0.40±0.09**	1.76±0.48	**0.73±0.26**	1.30±0.06	1.30

(d) The Accuracy Improvement (%) of NN models.

Method	D to B	E to B	K to B	B to D	E to D	K to D	B to E	D to E	K to E	B to K	D to K	E to K	Avg
SUP	0.44±0.10	8.66±0.02	14.10±0.02	0.01±0.10	3.79±0.05	7.96±0.03	2.29±0.10	1.31±0.10	2.04±0.01	1.52±0.07	1.95±0.06	0.54±0.02	3.72
DANN	-3.58±1.31	6.07±2.64	10.59±3.20	-1.91±0.81	0.77±1.69	2.17±2.19	-2.50±1.60	-1.93±1.42	0.21±0.72	-0.46±0.50	0.63±0.74	-1.35±0.75	0.73
DAN	-1.07±0.40	**7.94±0.59**	8.65±1.43	-1.13±0.55	**4.30±0.23**	**7.65±0.27**	1.07±1.05	0.21±0.38	-0.63±1.87	-0.26±0.48	-2.21±0.44	-1.05±0.70	1.96
MCD	-2.57±2.13	6.03±1.39	9.09±2.94	-0.52±0.42	-0.41±2.48	0.40±3.98	-2.29±1.37	-1.28±1.12	1.13±0.57	0.14±0.33	1.03±0.56	-1.33±1.37	0.78
HDA+ToAlign	-2.06±1.20	4.99±2.62	8.56±3.29	-1.17±1.42	1.19±1.41	5.20±1.72	-0.83±1.80	0.00±1.43	0.53±1.71	-0.38±1.19	0.79±0.75	-1.92±0.82	1.24
CORAL	**-0.38±0.00**	5.76±0.00	12.90±0.00	-0.35±0.00	2.51±0.00	7.30±0.00	-0.16±0.00	0.40±0.00	1.71±0.00	0.26±0.00	0.32±0.00	-1.10±0.00	2.43
OTLin	-4.02±0.00	5.51±0.00	10.41±0.00	-3.83±0.00	1.36±0.00	5.18±0.00	-1.18±0.00	-2.03±0.00	-1.62±0.00	-0.91±0.00	-1.12±0.00	-2.33±0.00	0.45
CDA	-1.07±0.03	7.47±0.04	**13.09±0.04**	-0.52±0.04	3.61±0.04	7.54±0.02	**2.11±0.02**	**1.22±0.02**	**1.76±0.03**	**0.87±0.02**	**1.24±0.03**	**-0.22±0.02**	**3.09**
SCDA	-0.76±0.10	5.72±0.40	11.29±0.13	**0.16±0.14**	2.35±0.16	6.20±0.08	0.64±0.19	0.23±0.21	1.75±0.06	-0.27±0.42	-0.33±0.98	-0.28±0.04	2.23

(e) Number of Adapted Features of GBDT and NN models.

Method	D to B	E to B	K to B	B to D	E to D	K to D	B to E	D to E	K to E	B to K	D to K	E to K	Avg
SCDA GBDT	3.1±0.8	4.9±2.7	3.8±2.6	4.8±2.1	3.7±1.5	6.2±2.9	5.5±1.1	8.0±2.4	6.1±2.8	5.6±1.5	8.8±3.5	4.5±0.9	5.4
SCDA NN	1.9±1.1	3.2±1.6	7.8±3.4	7.0±2.8	5.5±2.7	8.5±2.5	11.3±5.3	9.7±4.6	30.5±5.0	10.0±2.6	7.4±2.1	19.6±2.3	10.2

Table 7: Adaptation performances of Amazon review tasks.

(a) The log-loss improvement (%) of GBDT models.

Method	D-1 to M-1	D-2 to M-2	D-3 to M-3	D-4 to M-4	Avg
Confidence-based	8.85+-0.16	9.13+-0.27	6.87+-0.04	6.62+-0.08	7.87
SCDA	12.69±0.16	14.35±0.08	10.00±0.24	10.19±0.26	11.81
SCDA(2K)	**12.82±0.26**	**14.72±0.14**	**10.67±0.23**	**10.93±0.25**	**12.29**

(b) The log-loss improvement (%) of NN models.

Method	D-1 to M-1	D-2 to M-2	D-3 to M-3	D-4 to M-4	Avg
Confidence-based	7.52+-0.10	5.85+-0.21	10.01+-0.25	8.25+-0.05	7.91
SCDA	**11.84±0.25**	**8.85±0.87**	**19.56±0.46**	14.60±0.63	**13.71**
SCDA(2K)	11.40±1.33	6.88±0.85	18.95±0.41	**15.18±0.53**	13.10

(c) The PR_AUC improvement (%) of GBDT models.

Method	D-1 to M-1	D-2 to M-2	D-3 to M-3	D-4 to M-4	Avg
Confidence-based	0.07+-0.04	0.08+-0.16	0.04+-0.04	0.03+-0.04	0.05
SCDA	**2.15±0.08**	4.25±0.13	3.02±0.15	2.55±0.17	2.99
SCDA(2K)	2.01±0.32	**4.38±0.23**	**3.34±0.30**	**3.04±0.21**	**3.19**

(d) The PR_AUC improvement (%) of NN models.

Method	D-1 to M-1	D-2 to M-2	D-3 to M-3	D-4 to M-4	Avg
Confidence-based	-0.07+-0.07	-0.12+-0.15	-0.02+-0.11	-0.06+-0.05	-0.06
SCDA	**2.08±0.35**	**0.38±0.62**	**3.67±0.30**	2.50±0.35	**2.16**
SCDA(2K)	1.72±1.74	-0.15±0.58	3.23±0.55	**3.27±0.85**	2.02

Table 8: Performance comparison of the Kaggle fraud detection tasks between the confidence-based pseudo-labeling methods and the stability-based pseudo-labeling methods SCDA.

(a) The log-loss improvement (%) of GBDT models.

Method	Ger-1 to Bel-1	Ger-2 to Bel-2	Ger-3 to Bel-3	Avg
Confidence-based	3.90+-0.30	8.15+-0.95	**5.63+-1.34**	5.90
SCDA	**4.13±0.22**	**12.71±0.36**	5.42±0.99	**7.42**
SCDA(2K)	3.63±0.82	11.81±2.42	4.21±1.07	6.55

(b) The log-loss improvement (%) of NN models.

Method	Ger-1 to Bel-1	Ger-2 to Bel-2	Ger-3 to Bel-3	Avg
Confidence-based	-12.17+-0.74	1.43+-0.10	3.94+-0.99	-2.26
SCDA	**17.13±0.16**	**4.63±2.30**	**5.61±0.34**	**9.12**
SCDA(2K)	14.06±7.28	4.28±3.48	2.64±0.94	6.99

(c) The PR_AUC improvement (%) of GBDT models.

Method	Ger-1 to Bel-1	Ger-2 to Bel-2	Ger-3 to Bel-3	Avg
Confidence-based	**8.66+-1.62**	4.83+-6.66	-0.06+-0.43	4.48
SCDA	5.47±0.87	**13.24±1.91**	**0.76±0.77**	**6.49**
SCDA(2K)	3.77±0.77	12.44±6.37	0.65±2.74	5.62

(d) The PR_AUC improvement (%) of NN models.

Method	Ger-1 to Bel-1	Ger-2 to Bel-2	Ger-3 to Bel-3	Avg
Confidence-based	-1.29+-0.65	0.09+-0.06	0.09+-0.47	-0.37
SCDA	**24.38±0.53**	**4.09±0.70**	**1.96±1.63**	**10.15**
SCDA(2K)	19.44±10.39	1.00±3.19	-0.95±3.35	6.50

Table 9: Performance comparison of the real fraud detection tasks between the confidence-based pseudo-labeling methods and the stability-based pseudo-labeling methods SCDA.

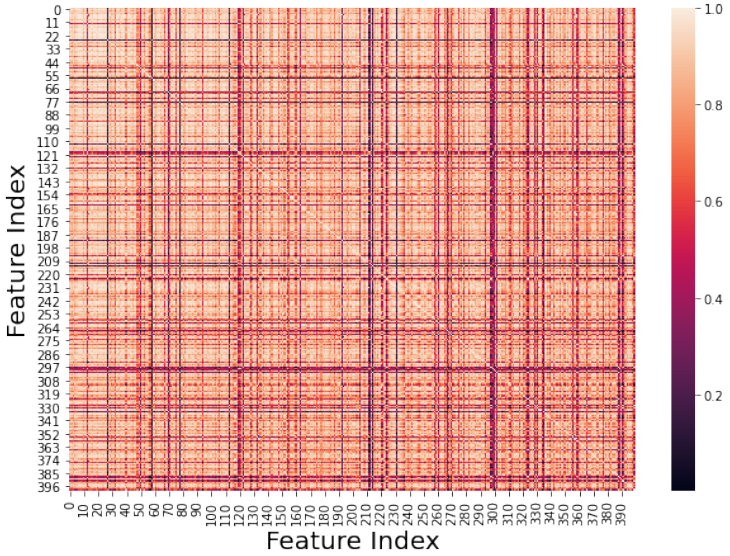

Figure 5: Absolute values of the correlation matrix of mSDA representations of Amazon reviews dataset (Electronics).

6.3 Ablation Study

This section aims first to disentangle how each step of the proposed SCDA method helps the adaptation (Recall that the three main steps of our method are illustrated by Figure 1) and then compare our proposed stability-based pseudo-labeling method to a confidence-based one.

We investigate the first question using GBDT models and the Kaggle fraud detection task, and we fix the number of source and target domain points to be 2,000. From the previously obtained empirical results, we know that this amount of data is sufficient to achieve good performances on Kaggle datasets. That is, we see in Table 2 that differences between SCDA and SCDA(2k) accuracies are marginal. Figure 6 illustrates the log-loss improvements of our proposition under three different settings: with full three steps, without the first step, and without the third step. Of note, one cannot solely eliminate the second step of our proposition, as the third step selects the adapted dimensions of the second step. We clearly see that all three steps of our proposition contribute to the DA. Eliminating one of them results in a decrease in adaptation performances. However, the impact of each step is different. Removing the label shift correction step has less impact than removing the feature selection step on the studied task.

Table 8 and Table 9 illustrate the performances of SCDA and a DA method using confidence-based pseudo-labels. The confidence-based DA method relies on the same coordinate-wise DA functions as SCDA, while the feature selection

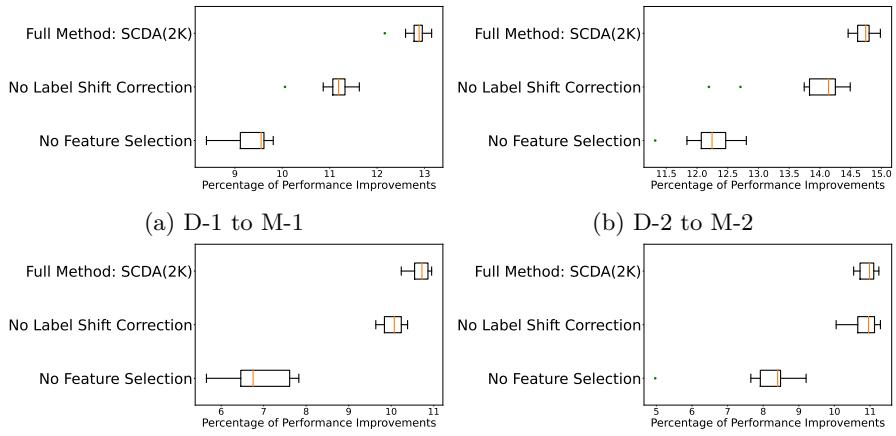

(a) D-1 to M-1

(b) D-2 to M-2

(c) D-3 to M-3

(d) D-4 to M-4

Figure 6: Ablation Study. The log-loss improvements of Kaggle fraud detection tasks with GBDT models. "Full Method: SCDA(2K)" represents our adaptation model with full 3 steps (see Figure 1). Whereas "No Label Shift Correction" skips the first step, and "No Feature Selection" skips the third step.

criterion is different. It considers predicted probabilities close to 0 (resp. 1) as negative examples (resp. positive examples), and a greedy algorithm is adopted to adapt dimensions that minimize prediction risks on such pseudo-labels. Compared to SCDA with stability-based pseudo-labels, the confidence-based method is shown to be less efficient in all cases of the Kaggle fraud detection tasks. In the real fraud detection tasks, SCDA also outperforms the confidence-based method on average with all families of models.

These two studies show that our proposed unsupervised feature selection method, which is one of the core contributions of this work, is well-suited for DA tasks.

6.4 Interpretability of Coordinate-wise Domain Adaptation with Greedy Feature Selection

Interpretability is one of our coordinate-wise optimal transport method assets compared to classical DA methods [18, 15]. For example, by investigating the obtained joint probability matrix γ^k of categorical features (Equation (11)), one can get mapping details between each modality. We show one example in Figure 7 where the mapping matrix of a categorical feature in the Kaggle dataset is illustrated. For this categorical feature, the source domain has more encoded value 0 than the one of the target domain; thus, by solving Equation (11), the encoded values 2 and 3 in the target domain have respectively 30.7% and 57.7% probability being mapped to the encoded value 0 in the source domain. Values of the Kaggle fraud detection dataset are masked for privacy protection. This

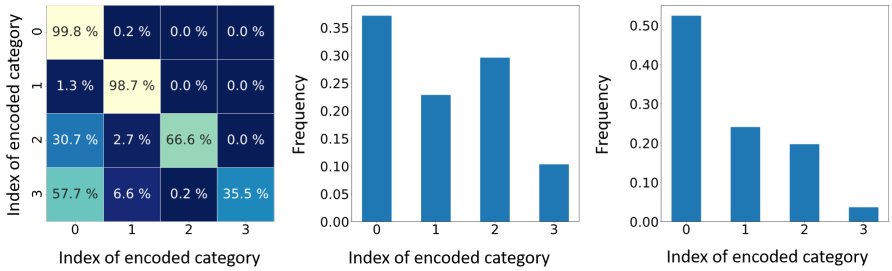

Figure 7: Left: The mapping matrix of a categorical feature where different values are encoded by integer numbers. Middle: The target domain distribution of this categorical feature. Right: The source domain distribution of this categorical feature.

example is obtained by using the general occurrence frequency distance [25], while a business-specific distance between categorical values can also be applied to fit different real-life industrial cases.

Moreover, the greedy feature selection process enhances this interpretability through the selected subset of features $\tilde{\alpha}_i$ and their selected orders. Specifically, the feature subset $\tilde{\alpha}_i$ reveals the source of drifts between source and target domains, and the order provides the importance of each feature in DA tasks intuitively. This information can provide business experts with insights to better interpret different domains. An example is illustrated in Figure 8, where the evolution of log-loss at each step of greedy feature selection is shown over the Kaggle payment dataset. The contribution of each feature can be measured by the differences in test risk. In this example, the contribution of the first adapted feature is significantly larger than the others. Consequently, one can investigate this feature to modelize customers' payment habits from different domains.

7 Conclusion

This paper proposed an unsupervised DA pipeline leveraging a feature selection process with a stability-based pseudo-label estimator to address the *target to source* DA problem for tabular data. The proposed method outperforms all compared *deep adaptation methods* and *classical adaptation methods* on average and is more stable facing various random states. Moreover, different from previous works that rely on tedious parameter fine-tuning or address only numerical features, our proposition (SCDA) is *model-agnostic*, *retraining-free*, and *feature-type independent*. In addition, the sparsity and orders of selected features by the unsupervised process can reveal the meaningful source of gaps between source and target domains. Although the proposed coordinate-wise adaptation function can be directly applied to multi-class classification problems,

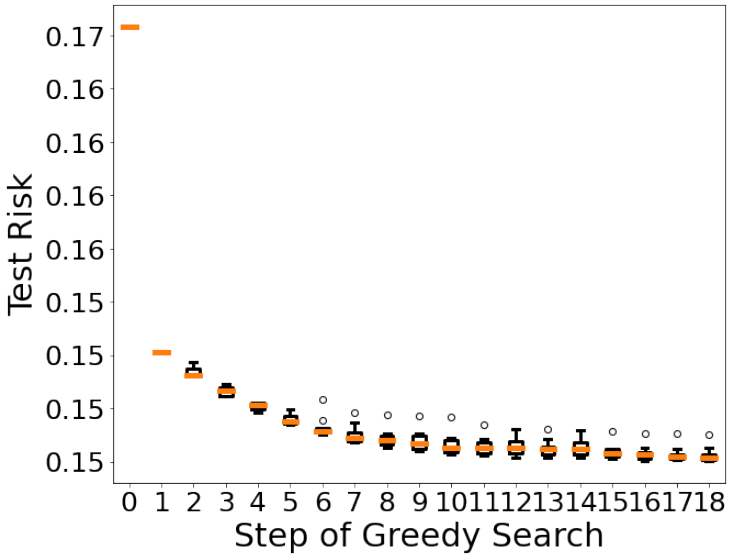

Figure 8: The evolution of log-loss risk at different steps of the greedy algorithm on Kaggle datasets in a supervised scenario. We repeat the feature selection process 10 times and report variations at each step by a box plot.

as discussed at the end of Section 4.2, the generalization of stability-based pseudo-labeling to multi-class classifications is not straightforward. To this end, we aim to leverage multi-class DA theories to further improve our proposition. Furthermore, we also aim to study the way of applying our proposition to a more challenging and generic universal DA problem. Note that our proposed pseudo-labeling technique can be easily generalized to other families of transformations; we aim to investigate its flexibility more formally over other adaptation functions besides optimal transports.

A Proof of Proposition 1

Proof. By the Bayes' theorem, we have

$$\begin{aligned}
&P(Y^p = y|X^p = x) \\
&= \frac{P(X^p = x|Y^p = y)P(Y^p = y)}{P(X^p = x)} \\
&= \frac{P(X^s = x|Y^s = y)P(Y^t = y)}{P(X^p = x)} \\
&= \frac{P(Y^s = y|X^s = x)P(Y^t = y)P(X^s = x)}{P(Y^s = y)P(X^p = x)} \\
&= P(Y^s = y|X^s = x)q(x)w(y)\,, \qquad (26)
\end{aligned}$$

where

$$q(x) = \frac{P(X^s = x)}{P(X^p = x)}\,.$$

As we have

$$\begin{aligned}
&\sum_y P(Y^p = y|X^p = x) = 1 \\
&\implies \sum_y P(Y^s = y|X^s = x)q(x)w(y) = 1\,,
\end{aligned}$$

solving the equation in $q(x)$ we get

$$q(x) = \left[\sum_y P(Y^s = y|X^s = x)w(y)\right]^{-1}\,.$$

We inject this solution into Equation (26) and we get

$$P(Y^p = y|X^p = x) = \frac{P(Y^s = y|X^s = x)w(y)}{\sum_{y'} P(Y^s = y'|X^s = x)w(y')}\,.$$

In a binary classification problem, y takes values in $\{0, 1\}$. Replacing $P(Y^p = y|X^p = x)$ and $P(Y^s = y|X^s = x)$ respectively by h_p and h_s proves Equation (5). □

References

[1] Mahsa Baktashmotlagh, Mehrtash T Harandi, Brian C Lovell, and Mathieu Salzmann. Unsupervised domain adaptation by domain invariant projection. In *ICCV*, pages 769–776, 2013.

[2] Shai Ben-David, John Blitzer, Koby Crammer, Fernando Pereira, et al. Analysis of representations for domain adaptation. *NIPS*, 19:137, 2007.

[3] John Blitzer, Ryan McDonald, and Fernando Pereira. Domain adaptation with structural correspondence learning. In *Conference on Empirical Methods in Natural Language Processing*, pages 120–128, 2006.

[4] Vadim Borisov, Tobias Leemann, Kathrin Seßler, Johannes Haug, Martin Pawelczyk, and Gjergji Kasneci. Deep neural networks and tabular data: A survey. *arXiv preprint arXiv:2110.01889*, 2021.

[5] Zhangjie Cao, Lijia Ma, Mingsheng Long, and Jianmin Wang. Partial adversarial domain adaptation. In *Proceedings of the European Conference on Computer Vision (ECCV)*, pages 135–150, 2018.

[6] Zhangjie Cao, Kaichao You, Mingsheng Long, Jianmin Wang, and Qiang Yang. Learning to transfer examples for partial domain adaptation. In *Proceedings of the IEEE/CVF Conference on Computer Vision and Pattern Recognition*, pages 2985–2994, 2019.

[7] Chao Chen, Zhihang Fu, Zhihong Chen, Sheng Jin, Zhaowei Cheng, Xinyu Jin, and Xian-Sheng Hua. Homm: Higher-order moment matching for unsupervised domain adaptation. In *AAAI*, volume 34, pages 3422–3429, 2020.

[8] Minmin Chen, Kilian Q Weinberger, and John Blitzer. Co-training for domain adaptation. In *NIPS*, pages 2456–2464, 2011.

[9] Minmin Chen, Zhixiang Eddie Xu, Kilian Q. Weinberger, and Fei Sha. Marginalized denoising autoencoders for domain adaptation. In *ICML*, 2012.

[10] Nicolas Courty, Rémi Flamary, Amaury Habrard, and Alain Rakotomamonjy. Joint distribution optimal transportation for domain adaptation. In *NIPS*, 2017.

[11] Nicolas Courty, Rémi Flamary, Devis Tuia, and Alain Rakotomamonjy. Optimal transport for domain adaptation. *IEEE Transactions on Pattern Analysis and Machine Intelligence*, 39(9):1853–1865, 2016.

[12] Shuhao Cui, Xuan Jin, Shuhui Wang, Yuan He, and Qingming Huang. Heuristic domain adaptation. *Advances in Neural Information Processing Systems*, 33:7571–7583, 2020.

[13] Shuhao Cui, Shuhui Wang, Junbao Zhuo, Chi Su, Qingming Huang, and Qi Tian. Gradually vanishing bridge for adversarial domain adaptation. In *Proceedings of the IEEE/CVF conference on computer vision and pattern recognition*, pages 12455–12464, 2020.

[14] Marco Cuturi. Sinkhorn distances: Lightspeed computation of optimal transport. In *NIPS*, 2013.

[15] Basura Fernando, Amaury Habrard, Marc Sebban, and Tinne Tuytelaars. Unsupervised visual domain adaptation using subspace alignment. In *ICCV*, pages 2960–2967, 2013.

[16] R'emi Flamary and Nicolas Courty. Pot python optimal transport library, 2017.

[17] Geoffrey French, Michal Mackiewicz, and Mark Fisher. Self-ensembling for visual domain adaptation. February 2018. ICLR.

[18] Yaroslav Ganin, Evgeniya Ustinova, Hana Ajakan, Pascal Germain, Hugo Larochelle, François Laviolette, Mario Marchand, and Victor Lempitsky. Domain-adversarial training of neural networks. *JMLR*, 17(1):2096–2030, 2016.

[19] Léo Gautheron, Ievgen Redko, and Carole Lartizien. Feature selection for unsupervised domain adaptation using optimal transport. In *ECML PKDD*, pages 759–776. Springer, 2018.

[20] Mingming Gong, Kun Zhang, Tongliang Liu, Dacheng Tao, Clark Glymour, and Bernhard Schölkopf. Domain adaptation with conditional transferable components. In *ICML*, pages 2839–2848. PMLR, 2016.

[21] Ian Goodfellow, Jean Pouget-Abadie, Mehdi Mirza, Bing Xu, David Warde-Farley, Sherjil Ozair, Aaron Courville, and Yoshua Bengio. Generative adversarial nets. 27, 2014.

[22] James J Heckman. Sample selection bias as a specification error. *Econometrica: Journal of the Econometric Society*, pages 153–161, 1979.

[23] Jiaxing Huang, Dayan Guan, Aoran Xiao, and Shijian Lu. Model adaptation: Historical contrastive learning for unsupervised domain adaptation without source data. *Advances in Neural Information Processing Systems*, 34, 2021.

[24] Nathalie Japkowicz and Shaju Stephen. The class imbalance problem: A systematic study. *Intelligent data analysis*, 6(5):429–449, 2002.

[25] Karen Sparck Jones. A statistical interpretation of term specificity and its application in retrieval. *Journal of documentation*, 1972.

[26] Leonid Kantorovich. On the translocation of masses. *Management Science*, 5(1):1–4, 1958.

[27] Guolin Ke, Qi Meng, Thomas Finley, Taifeng Wang, Wei Chen, Weidong Ma, Qiwei Ye, and Tie-Yan Liu. Lightgbm: A highly efficient gradient boosting decision tree. *NIPS*, 30:3146–3154, 2017.

[28] Jogendra Nath Kundu, Naveen Venkat, R Venkatesh Babu, et al. Universal source-free domain adaptation. In *Proceedings of the IEEE/CVF Conference on Computer Vision and Pattern Recognition*, pages 4544–4553, 2020.

[29] Vinod K Kurmi, Venkatesh K Subramanian, and Vinay P Namboodiri. Domain impression: A source data free domain adaptation method. In *WACV*, pages 615–625, 2021.

[30] Dong-Hyun Lee. Pseudo-label: The simple and efficient semi-supervised learning method for deep neural networks. In *Workshop on challenges in representation learning, ICML*, volume 3, 2013.

[31] Guangrui Li, Guoliang Kang, Yi Zhu, Yunchao Wei, and Yi Yang. Domain consensus clustering for universal domain adaptation. In *Proceedings of the IEEE/CVF Conference on Computer Vision and Pattern Recognition*, pages 9757–9766, 2021.

[32] Jingjing Li, Zhekai Du, Lei Zhu, Zhengming Ding, Ke Lu, and Heng Tao Shen. Divergence-agnostic unsupervised domain adaptation by adversarial attacks. *IEEE Transactions on Pattern Analysis and Machine Intelligence*, 2021.

[33] Jingjing Li, Mengmeng Jing, Hongzu Su, Ke Lu, Lei Zhu, and Heng Tao Shen. Faster domain adaptation networks. *IEEE Transactions on Knowledge and Data Engineering*, 2021.

[34] Rui Li, Qianfen Jiao, Wenming Cao, Hau-San Wong, and Si Wu. Model adaptation: Unsupervised domain adaptation without source data. In *Proceedings of the IEEE/CVF Conference on Computer Vision and Pattern Recognition*, pages 9641–9650, 2020.

[35] Jian Liang, Dapeng Hu, and Jiashi Feng. Do we really need to access the source data? source hypothesis transfer for unsupervised domain adaptation. In *ICML*, pages 6028–6039. PMLR, 2020.

[36] Jian Liang, Dapeng Hu, Jiashi Feng, and Ran He. Dine: Domain adaptation from single and multiple black-box predictors. In *Proceedings of the IEEE/CVF Conference on Computer Vision and Pattern Recognition*, 2022.

[37] Yi Lin, Yoonkyung Lee, and Grace Wahba. Support vector machines for classification in nonstandard situations. *Machine learning*, 46(1-3):191–202, 2002.

[38] Zachary Lipton, Yu-Xiang Wang, and Alexander Smola. Detecting and correcting for label shift with black box predictors. In *International conference on machine learning*, pages 3122–3130. PMLR, 2018.

[39] Xiaofeng Liu, Zhenhua Guo, Site Li, Fangxu Xing, Jane You, C-C Jay Kuo, Georges El Fakhri, and Jonghye Woo. Adversarial unsupervised domain adaptation with conditional and label shift: Infer, align and iterate. In *Proceedings of the IEEE/CVF International Conference on Computer Vision*, pages 10367–10376, 2021.

[40] Mingsheng Long, Yue Cao, Jianmin Wang, and Michael I. Jordan. Learning transferable features with deep adaptation networks. In *ICML*, 2015.

[41] Mingsheng Long, Zhangjie Cao, Jianmin Wang, and Michael I Jordan. Conditional adversarial domain adaptation. In *NeurIPS*, pages 1640–1650, 2018.

[42] Mingsheng Long, Jianmin Wang, Guiguang Ding, Jiaguang Sun, and Philip S Yu. Transfer feature learning with joint distribution adaptation. In *ICCV*, 2013.

[43] Mingsheng Long, Han Zhu, Jianmin Wang, and Michael I Jordan. Deep transfer learning with joint adaptation networks. In *ICML*, pages 2208–2217. PMLR, 2017.

[44] Gaspard Monge. Mémoire sur la théorie des déblais et des remblais. *Histoire de l'Académie Royale des Sciences de Paris*, 1781.

[45] Saeid Motiian, Quinn Jones, Seyed Iranmanesh, and Gianfranco Doretto. Few-shot adversarial domain adaptation. In I. Guyon, U. V. Luxburg, S. Bengio, H. Wallach, R. Fergus, S. Vishwanathan, and R. Garnett, editors, *NeurIPS*, volume 30. Curran Associates, Inc., 2017.

[46] Sinno Jialin Pan, Ivor W Tsang, James T Kwok, and Qiang Yang. Domain adaptation via transfer component analysis. *IEEE Transactions on Neural Networks*, 22(2):199–210, 2010.

[47] Sinno Jialin Pan and Qiang Yang. A survey on transfer learning. *IEEE Transactions on Knowledge and Data Engineering*, 22(10):1345–1359, 2009.

[48] Pau Panareda Busto and Juergen Gall. Open set domain adaptation. In *Proceedings of the IEEE international conference on computer vision*, pages 754–763, 2017.

[49] Adam Paszke, Sam Gross, Francisco Massa, Adam Lerer, James Bradbury, Gregory Chanan, Trevor Killeen, Zeming Lin, Natalia Gimelshein, Luca Antiga, et al. Pytorch: An imperative style, high-performance deep learning library. In *NeurIPS*, volume 32, pages 8026–8037. Curran Associates, Inc., 2019.

[50] Michaël Perrot, Nicolas Courty, Rémi Flamary, and Amaury Habrard. Mapping estimation for discrete optimal transport. In *NIPS*, pages 4204–4212, 2016.

[51] Gabriel Peyré and Marco Cuturi. Computational optimal transport. *Foundations and Trends in Machine Learning*, 11(5-6):355–607, 2019.

[52] Ievgen Redko, Nicolas Courty, Rémi Flamary, and Devis Tuia. Optimal transport for multi-source domain adaptation under target shift. In *The 22nd International Conference on Artificial Intelligence and Statistics*, pages 849–858. PMLR, 2019.

[53] Marco Saerens, Patrice Latinne, and Christine Decaestecker. Adjusting the outputs of a classifier to new a priori probabilities: a simple procedure. *Neural computation*, 14(1):21–41, 2002.

[54] Kuniaki Saito, Yoshitaka Ushiku, and Tatsuya Harada. Asymmetric tri-training for unsupervised domain adaptation. In *ICML*, 2017.

[55] Kuniaki Saito, Kohei Watanabe, Yoshitaka Ushiku, and Tatsuya Harada. Maximum classifier discrepancy for unsupervised domain adaptation. In *CVPR*, pages 3723–3732, 2018.

[56] Kuniaki Saito, Shohei Yamamoto, Yoshitaka Ushiku, and Tatsuya Harada. Open set domain adaptation by backpropagation. In *Proceedings of the European Conference on Computer Vision (ECCV)*, pages 153–168, 2018.

[57] Sandeepkumar Satpal and Sunita Sarawagi. Domain adaptation of conditional probability models via feature subsetting. In *ECML PKDD*, pages 224–235. Springer, 2007.

[58] Hidetoshi Shimodaira. Improving predictive inference under covariate shift by weighting the log-likelihood function. *Journal of Statistical Planning and Inference*, 90(2):227–244, 2000.

[59] Rui Shu, Hung H. Bui, Hirokazu Narui, and Stefano Ermon. A DIRT-T approach to unsupervised domain adaptation. In *ICLR*. OpenReview.net, 2018.

[60] Masashi Sugiyama, Shinichi Nakajima, Hisashi Kashima, Paul V Buenau, and Motoaki Kawanabe. Direct importance estimation with model selection and its application to covariate shift adaptation. In *NIPS*, 2008.

[61] Baochen Sun, Jiashi Feng, and Kate Saenko. Correlation alignment for unsupervised domain adaptation. In *Domain Adaptation in Computer Vision Applications*, pages 153–171. Springer, 2017.

[62] Remi Tachet des Combes, Han Zhao, Yu-Xiang Wang, and Geoffrey J Gordon. Domain adaptation with conditional distribution matching and generalized label shift. *Advances in Neural Information Processing Systems*, 33:19276–19289, 2020.

[63] Antonio Torralba and Alexei A Efros. Unbiased look at dataset bias. In *CVPR*, pages 1521–1528. IEEE, 2011.

[64] Yun-Yun Tsai, Pin-Yu Chen, and Tsung-Yi Ho. Transfer learning without knowing: Reprogramming black-box machine learning models with scarce data and limited resources. In *International Conference on Machine Learning*, pages 9614–9624. PMLR, 2020.

[65] Eric Tzeng, Judy Hoffman, Kate Saenko, and Trevor Darrell. Adversarial discriminative domain adaptation. In *CVPR*, pages 7167–7176, 2017.

[66] Selen Uguroglu and Jaime Carbonell. Feature selection for transfer learning. In *ECML PKDD*, pages 430–442. Springer, 2011.

[67] Riccardo Volpi, Pietro Morerio, Silvio Savarese, and Vittorio Murino. Adversarial feature augmentation for unsupervised domain adaptation. In *Proceedings of the IEEE conference on computer vision and pattern recognition*, pages 5495–5504, 2018.

[68] Qian Wang and Toby Breckon. Unsupervised domain adaptation via structured prediction based selective pseudo-labeling. In *AAAI Conference on Artificial Intelligence*, volume 34, pages 6243–6250, 2020.

[69] Guoqiang Wei, Cuiling Lan, Wenjun Zeng, and Zhibo Chen. Metaalign: Coordinating domain alignment and classification for unsupervised domain adaptation. In *Proceedings of the IEEE/CVF Conference on Computer Vision and Pattern Recognition*, pages 16643–16653, 2021.

[70] Guoqiang Wei, Cuiling Lan, Wenjun Zeng, Zhizheng Zhang, and Zhibo Chen. Toalign: Task-oriented alignment for unsupervised domain adaptation. *Advances in Neural Information Processing Systems*, 34, 2021.

[71] Yi Yang, Yueting Zhuang, and Yunhe Pan. Multiple knowledge representation for big data artificial intelligence: framework, applications, and case studies. *Frontiers of Information Technology & Electronic Engineering*, 22(12):1551–1558, 2021.

[72] Hao-Wei Yeh, Baoyao Yang, Pong C Yuen, and Tatsuya Harada. Sofa: Source-data-free feature alignment for unsupervised domain adaptation. In *WACV*, pages 474–483, 2021.

[73] Jason Yosinski, Jeff Clune, Yoshua Bengio, and Hod Lipson. How transferable are features in deep neural networks? In *NIPS*, pages 3320–3328, 2014.

[74] Kaichao You, Mingsheng Long, Zhangjie Cao, Jianmin Wang, and Michael I Jordan. Universal domain adaptation. In *Proceedings of the IEEE/CVF conference on computer vision and pattern recognition*, pages 2720–2729, 2019.

[75] Kaichao You, Ximei Wang, Mingsheng Long, and Michael Jordan. Towards accurate model selection in deep unsupervised domain adaptation. In *ICML*, pages 7124–7133. PMLR, 2019.

[76] Werner Zellinger, Thomas Grubinger, Edwin Lughofer, Thomas Natschläger, and Susanne Saminger-Platz. Central moment discrepancy (cmd) for domain-invariant representation learning. 04 2017.

[77] Haojian Zhang, Yabin Zhang, Kui Jia, and Lei Zhang. Unsupervised domain adaptation of black-box source models. *arXiv preprint arXiv:2101.02839*, 2021.

[78] Luxin Zhang, Pascal Germain, Yacine Kessaci, and Christophe Biernacki. Target to source coordinate-wise adaptation of pre-trained models. In *ECML PKDD*, pages 378–394. Springer International Publishing, 2021.

[79] Yabin Zhang, Bin Deng, Hui Tang, Lei Zhang, and Kui Jia. Unsupervised multi-class domain adaptation: Theory, algorithms, and practice. *IEEE Transactions on Pattern Analysis and Machine Intelligence*, 2020.

[80] Yuchen Zhang, Tianle Liu, Mingsheng Long, and Michael Jordan. Bridging theory and algorithm for domain adaptation. In *International Conference on Machine Learning*, pages 7404–7413. PMLR, 2019.

[81] Xiaojin Jerry Zhu. Semi-supervised learning literature survey. Technical report, University of Wisconsin-Madison Department of Computer Sciences, 2005.